UAlg
UNIVERSIDADE DO ALGARVE

UNIVERSIDADE DO ALGARVE
INSTITUTO SUPERIOR DE ENGENHARIA

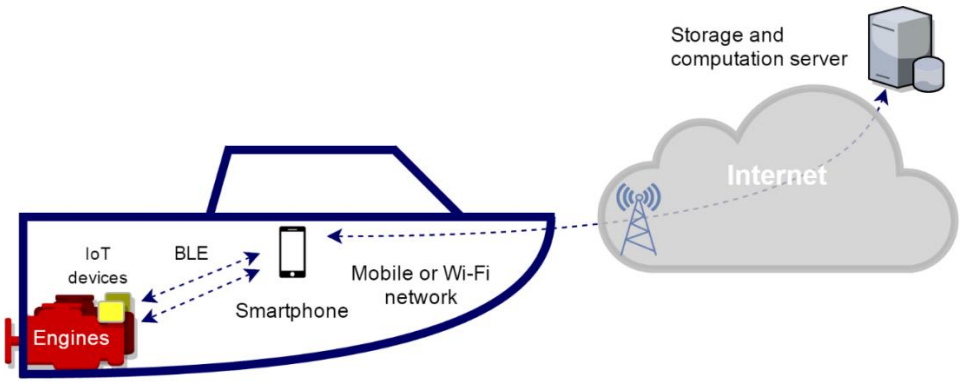

FAULT DETECTION SYSTEM FOR INTERNAL COMBUSTION ENGINES

SISTEMA DE DETEÇÃO DAS FALHAS PARA MOTORES DE COMBUSTÃO INTERNA

Sergey Nogin

Dissertação para a obtenção do grau de Mestre em
Engenharia Eléctrica e Electrónica
Especialização em Tecnologias de Informação e Telecomunicações

Orientador: Professor Doutor Jânio Miguel E. Ferreira Monteiro
Orientador: Professor Doutor Jorge Filipe Leal Costa Semião

Junho, 2017

Title: Fault detection system for internal combustion engines
Título: Sistema de Deteção das Falhas para motores de Combustão Interna

Authorship: Sergey Nogin
Autor: Sergey Nogin

I hereby declare to be the author of this original and unique work. Authors and references in use are properly cited in the text and are all listed in the reference section.

Declaro ser o autor deste trabalho, que é original e inédito. Autores e trabalhos consultados estão devidamente citados no texto e constam da listagem de referências incluída.

_____

Sergey Nogin

Dedicated to my parents.

ACKNOWLEDGMENTS

I would like to thank my thesis advisors, Prof. Jânio Monteiro and Jorge Semião for all support provided during the elaboration of this dissertation and study process.

I would like to thank Mauro Bomtempo, Prof. Nelson Sousa and Henrique Catarino for the help in conducting practical experiments.

Sergey Nogin, Faro, June 30th, 2017

RESUMO

O desenvolvimento de dispositivos para Internet das Coisas abre novas oportunidades na área de manutenção preditiva. A ideia geral da Internet das Coisas é ligar tudo à Internet, permitindo criar assim sistemas escaláveis suportados pelo processamento remoto, centralizado ou decentralizado. Com a utilização de módulos de baixa potência e de baixo custo, esses sistemas são também eficazes em termos de custo.

Alguns estudos indicam que nos próximos anos a manutenção preditiva das máquinas será a principal aplicação da análise de dados na indústria, baseada em Internet das Coisas. Apesar de existirem vários tipos de máquinas, as mais importantes são os motores elétricos e os de combustão interna. Os motores elétricos são amplamente utilizados em diversos setores. Já os motores de combustão interna, por sua vez, são principalmente utilizados nas indústrias automóvel e marítima.

Tipicamente, os motores modernos de combustão interna têm uma unidade de controlo computadorizado com capacidade de autodiagnóstico. Contudo, ao contrario da indústria automóvel que utiliza o sistema de *On-board diagnostics*, a indústria marítima não possui uma norma definida, ou pelo menos uma norma dominante. Isso acarreta a utilização de equipamentos de preço elevado para extrair informação sobre o estado do motor da unidade de controlo. Além disso, a monitorização é intermitente, obrigando ao proprietário de uma embarcação a efetuar a extração dos dados periodicamente para posterior análise.

A monitorização das características de operação de um motor um processo fundamental numa manutenção preditiva, sendo que, pela monitorização de um ou mais parâmetros de uma máquina (incluindo a vibração, temperatura, etc.), tenta identificar uma mudança significativa na mesma, que, por sua vez, possa indicar o aparecimento de uma falha. A estratégia de monitorização preditiva assegura que as atividades de manutenção são executadas apenas quando são realmente necessárias, mas para tal é necessário monitorizar periodicamente ou constantemente o equipamento, processar os dados e analisar os resultados. Este método tem, no entanto, as suas desvantagens. O custo do equipamento portátil de monitorização, ou de um sistema estacionário que esteja permanentemente instalado, depende do tipo de variáveis monitorizadas, da precisão de medida, do ambiente de trabalho, ou até do nível de desenvolvimento do sistema. Para além disso, o defeito pode não ser detetado, ou então ser detetado um defeito não existente (um falso positivo, ou uma falsa detecção).

Para efectuar uma monitorização preditiva, podem ser utilizados um ou mais métodos de monitorização. Os métodos principais são: análise de vibração, análise de óleo, análise de desempenho, termografia, ferrografia ou análise dos sinais acústicos. De entre todos, a análise de vibração é particularmente interessante, por ser um método não intrusivo e por permitir não só detetar as falhas, mas também classificá-las. Para monitorizar as vibrações de uma máquina utilizam-se transdutores de deslocamento, de velocidade ou de aceleração (acelerómetros). Os transdutores de deslocamento utilizados na indústria permitem medir apenas o deslocamento relativo, o que nem sempre é conveniente. Os preços dos transdutores industriais de velocidade são relativamente altos. Os acelerómetros piezoelétricos industrias também têm um preço elevado. Se as condições ambientais não forem exageradas (por exemplo, temperaturas elevadas) podem ser utilizados acelerómetros MEMS (*Microelectromechanical system*). Os acelerómetros do tipo MEMS não têm a resposta em frequência tão ampla como os piezoelétricos, no entanto a diferença de preço em relação às restantes opções é muito significativa, e os acelerómetros MEMS, hoje em dia, são praticamente todos digitais, o que simplifica o sistema. Outra alternativa é a película piezoelétrica feita a partir de *polyvinylidene difluoride* (PVDF). A resposta em frequência desta pelicula é por vezes melhor do que a dos acelerómetros piezoelétricos, com frequências de ressonância acima de 10 MHz. O preço de uma película PVDF depende das dimensões da película, mas é normalmente maior do que o preço de um acelerómetro MEMS, sendo ainda assim muito menor do que um acelerómetro piezoelétrico. É importante referir que há modelos de acelerômetros piezoelétricos que incluem amplificador, mas no caso da película PVDF requerem um circuito de condicionamento do sinal. Para além disso, no caso da película PVDF, tem que ser considerada a sensibilidade à interferência eletromagnética.

Dado este contexto, o trabalho realizado nesta Tese resulta de uma proposta feita por uma empresa interessada em automatizar este processo, que entrou em contato com universidade para encontrar uma possível solução. O sistema desenvolvido baseia-se no conceito Internet das Coisas, efetuando a monitorização autónoma da condição do motor, de forma independente do sistema de autodiagnóstico que possa existir.

Este trabalho tem, genericamente, três objetivos: (i) desenvolver um módulo de contabilização do número de horas de funcionamento do motor; (ii) desenvolver um módulo de monitorização de ocorrência de falhas num motor de combustão interna através da medição e análise de vibrações; (iii) investigar e analisar os resultados de monitorização, para identificar desvios de parâmetros de funcionamento e detetar de forma preditiva a ocorrência de falhas (antes que as mesmas ocorram realmente).

O sistema, que compreende os módulos (i) e (ii), será montado no motor, comunicando com um dispositivo do cliente (por exemplo, um smartphone ou tablet) através de uma interface sem fios. Neste caso optou-se por utilizar uma ligação sem fios baseada na tecnologia *Bluetooth Low Energy*.

Para implementação do módulo de contabilização do número de horas de funcionamento, recorreu-se a um sensor do tipo MEMS, por ter um consumo muito baixo. Já o módulo de módulo de monitorização de ocorrência de falhas recorre a um sensor do tipo PVDF, por permitir elevadas definições temporais na captura do sinal de vibração.

Para efectuar a análise de dados que permite a identificação da ocorrência de falhas, foram testados e comparados um conjunto de 16 algoritmos de análise conjunta de dados no tempo e na frequência, suportando a identificação de falhas e a diferenciação entre tipos de falhas. Os algoritmos foram avaliados com base em dados reais, obtidos por falhas induzidas num motor de combustão interna, permitindo por essa via encontrar os algoritmos que melhor servem o objetivo proposto.

PALAVRAS-CHAVE: Internet das Coisas, Deteção de Faltas, Motores de Combustão Interna, Análise Tempo-Frequência.

ABSTRACT

The purpose of this work is to develop a non-intrusive low-cost system capable of detecting faults and register working hours of Internal Combustion (IC) engines. The system should allow the monitoring of combustion engines usage, detect faults remotely, and is focused on IC engines for maritime applications. As explained in the following it consists of two parts. The first part involves the development of the device, which should be capable of performing a continuous monitoring of an engine's activity and register its working periods. This decision is made based on the vibration analysis. As a requirement, the developed device must be low-cost, portable and have a low energy consumption to provide at least two years of autonomy. The second part involves fault's detection and, like the first part, it requires information from the engine's vibrations. A low power accelerometer will be used to monitor the engine's activity, and a piezoelectric polyvinylidene fluoride film is used to record the engine's vibration, for fault detection. The data is then sent via Bluetooth to the user's smartphone, which forwards it to the Internet, for further analysis. Bluetooth Low Energy is used to support the required autonomy. The developed technique for fault detection includes data acquisition, analog and digital pre-processing, and digital processing. The most important part of the digital processing, in this case, is a Time-Frequency Analysis. Several Time-Frequency Analysis algorithms were tested with real data to select the best solution to detect faults in such engines.

KEYWORDS: Internet of Things, Fault detection, internal combustion engine, time-frequency analysis.

TABLE OF CONTENTS

LIST OF FIGURES

LIST OF TABLES

ACRONYMS

IoT	Internet of Things
ECU	Engine Control Unit
OBD	On-board diagnostics
IC	Internal Combustion
PVDF	Polyvinylidene fluoride
BLE	Bluetooth Low Energy
API	Application Programming Interface
M2M	Machine-to-Machine Communication
HMI	Human-Machine Interface
TFA	Time-Frequency Analysis
MEMS	Microelectromechanical system
EMI	Electromagnetic Interference
FFT	Fast Fourier Transform
TF	Time-frequency
ARMA	Auto-Regressive Moving Average
STFT	Short-time Fourier transform
CWT	Continuous Wavelet Transform
DWT	Discrete Wavelet Transform
WV	Wigner-Ville
WVD	Wigner-Ville distribution
PWVD	Pseudo-WVD
SPWVD	Smoothed-pseudo WVD
ZAMD	Zhao-Atlas-Marks distribution
IrDA	Infrared Data Association
NFC	Near-field communication
BR	Basic Rate

EDR	Enhanced Data Rate
LE	Low Energy
COAP	Constrained Application Protocol
MQTT	Message Queuing Telemetry Transport
HTTP	Hypertext Transfer Protocol
TI	Texas Instruments
MCU	Microcontroller unit
RF	Radio Frequency
EEPROM	Erasable Programmable Read-Only Memory
NVRAM	Non-Volatile Random-Access Memory
F-Ram	Ferroelectric Random-Access Memory
RTC	Real-Time Clock
ODR	Output data rate
I2C	Inter-Integrated Circuit
SPI	Serial Peripheral Interface
MRAM	Magnetoresistive random access memory
IDE	Integrated Development Environment
PMU	Power Management Unit
PPI	Programmable peripheral interconnect
SDK	Software development kit
GUI	Graphical user interface
ISR	Interrupt Service Routine
JFET	Junction gate field-effect transistor
Op-amp	Operational amplifier
PCB	Printed Circuit Board
RPM	Revolutions per minute

1. INTRODUCTION

Considering the typical maintenance strategies for a machine, there are four options to consider: (1) run to failure, (2) preventive maintenance, (3) predictive maintenance, and (4) proactive maintenance. In the case of the first strategy (i.e. run to failure), the engine runs until there is a fault. The repair is done or the damaged components are replaced when a complete stop of the engine occurs (or just before). The advantage is that the engine components run to the end of their life cycle, and the engine is withdrawn from service only when repair is really necessary. However, the disadvantage of this strategy is that it may likely cause significant damage to the engine. In addition, the process of buying and/or replacing the component that caused the breakdown can take a significant amount of time and, during this time, the engine will not be working [1][2].

In the case of a preventive maintenance strategy, the management or replacement of the engine elements is performed periodically using the recommendations of the engine manufacturers. The advantage of this method is that it typically avoids significant damage to the machine. The disadvantage is that the period between maintenance activities results from a typical average value and it may happen that, in some cases, maintenance can be done later, lowering costs, while in other cases, it should be done earlier [1].

The predictive maintenance strategy solves these previous problems because maintenance activities are performed only when they are really needed. In this case, it is necessary to periodically or constantly monitor the equipment, process the data and analyze the results. This method has, however, disadvantages. The cost of the portable monitoring equipment or a stationary monitoring system depends on the type of monitored variables, accuracy, working environment and system's development state. In addition, the defect may not be detected, or a non-existent defect may be detected. System adjustments and monitoring can be carried out by qualified technicians [2].

The proactive maintenance strategy, involves both preventive and predictive strategies, along with a mechanism that attempts to detect the source of failure. Typically, it uses a stationary system that monitors several parameters. In addition to detecting the fault, it ensures that the repair was appropriate and advises the user in case of needing to modify or change the

equipment. The advantages and disadvantages are generally the same: thorough monitoring of the equipment. This strategy minimizes failures and increases machine reliability. However, this is a high complex monitoring system, and it requires high qualification technicians to handle the specific monitoring equipment [2].

Choosing the appropriate maintenance strategy to use is done by analyzing the criticality of the system and also the economic factors [2]. Nowadays, run to failure and preventive strategies are becoming obsolete, while the predictive strategy is starting to be widely used. Regarding the proactive maintenance strategies, although very promising for the future, they have still a long way to go in order to be widely adopted.

In the case of predictive or proactive strategies, one or more monitoring methods may be used. The main methods are vibration analysis, oil analysis, performance analysis, thermography, ferrography or acoustic signal analysis [3]. From these methods, vibration analysis is particularly interesting, because it is a non-intrusive method and because it allows not only to detect the faults but also to classify them [4].

1.1 MOTIVATION

As stated in [1], Condition Monitoring is a major component of a predictive maintenance process that, by monitoring a parameter of machinery (including vibration, temperature, etc.), tries to identify a significant change, which is indicative of a developing fault.

The development of the Internet of Things (IoT) devices and concept opens up new opportunities in the field of such predictive maintenance. The idea of IoT is to connect everything to the Internet, and it allows the creation of scalable systems, supported by a centralized or distributed data processing. Due to the use of low-power and low-cost modules these systems are also cost effective.

According to [5], in the next few years, the predictive maintenance of machinery will be the main application of Industrial Analytics based on IoT. Machinery involves various kinds of machines, however, due to their prevalence, the most important machines are electrical motors and Internal Combustion (IC) engines. Electrical motors are broadly used in many different sectors. IC engines are extensively employed in the automotive and marine industry.

Modern marine IC engines have a computerized engine control unit (ECU) which generally has a self-diagnostic capability. However, different from the On-board diagnostics (OBD) of

the automotive industry, in marine systems, there is no dominant standard, and expensive equipment is required to retrieve the information about the engine's condition from the ECU. Also, the monitoring is intermittent, with the boat's owner needing to make periodic data retrieval and analysis.

Given this context, the work done in this Thesis results from a proposal made by a company that is interested in automating this process, which has contacted the university to find a possible solution. The developed system uses the IoT approach for autonomous monitoring of the engine's condition without using the self-diagnostic mechanism of the ECU.

1.2 OBJECTIVES

The purpose of this work is to develop a non-intrusive low-cost system capable of detecting faults and register working hours of IC engines. The main objectives state that the system should allow the monitoring of combustion motors usage, detect faults remotely, and is focused on IC engines for maritime applications. Therefore, this work consists of two parts, as explained in the following. The first part involves the development of the device, which should be capable of performing a continuous monitoring of an engine's activity and register its working periods. This monitoring is made based on the analysis of vibration. The second part involves faults' detection and, like the first part, requires information from the engine's vibrations. As additional objectives, the developed device must be low-cost, portable and have a low energy consumption to provide at least two years of autonomy.

1.3 DISSERTATION OVERVIEW

The dissertation is divided into six chapters. This chapter is dedicated to introduce the problem, describe the objectives and motivation of the work, as well as the structure of the dissertation.

In the following chapter, the state of the art concerning the working principle of hour meters, faults detection in IC engines and the options for wireless connectivity of IoT devices is presented.

The third chapter describes the selection process of components and sensors. It begins with the description of the system architecture and the architecture of the device used for the engine monitoring. Then, the main components are selected for each block of the described architecture.

In chapter four, the prototypes of the hour meter and the condition monitoring units are described. It starts by describing the schematic which is based on a modified system architecture, and previously selected components. It then describes the hour meter prototype. After describing the hardware part, the logic of the device firmware is explained. It begins with the description of the Bluetooth Low Energy (BLE) service designed to provide the interface with the hour meter block. Two types of calibration required for the normal operation of this block are explained next. Then the firmware algorithm is described. The consumption is evaluated in the end.

Chapter five begins with the description of the data acquisition system. In the following, the variation of vibration signal according with the rotational speed of the crankshaft is studied. Experimental conditions are described next, together with the description of the faults caused by the IC engine and used to evaluate the performance of different Time Frequency (TF) methods. In the next sub-chapter the results of the tests are presented, and the performance of the TF methods are compared based on the variation of Rényi information for different conditions.

In the last chapter, the conclusions are drawn and the future work is described.

2. STATE OF ART

In order to perform a continuous condition monitoring of engines, maintenance procedures need to be combined with communication technologies.

Maintenance procedures can either be classified in preventive or predictive methods. In terms of preventive procedures, they depend on the equipment's usage, which therefore needs to be measured. This approach, however, cannot assure unexpected failures, which may happen between preventing interventions. Predictive strategies, on the other hand, are based on regular condition monitoring and thus allow the detection of faults on their early stages [6], avoiding breakdown.

In the following, the description of some of the work done in both strategies is provided. It starts by describing the working principle for different types of hour meters, needed in preventive strategies. Afterward the state-of-the-art in fault detection for internal combustion engines is described. The implemented device can be used in predictive strategies. Finally, in the last subchapter, the communication solutions that can be used to transmit these data to an Internet based server are described.

2.1 HOUR METER

An hour meter is a device used to count the running time. Maintenance procedures of engines are many times based on this information. In the case of the marine engines, construction equipment like cranes or bulldozers, diesel generator or turbine generators, the estimation of the equipment's condition is done based on their working hours rather than in odometer readings. This is because the movement on the ground of this machinery is not the main work that they do [7].

Hour meters could be differentiated into three main types, according to with the kind of connection they require.

The first types are based on devices connected to some critical switching circuitry, for example, to an engine's kill switch [8]. Because the engine's status depends on the switch

position, this type of hour meter is simple and reliable. However, it is intrusive, and the understanding of the ignition system or at least of the switch circuit is required in order to install the device properly.

The second type of devices identify the state of the engines, either using a capacitive or an inductive pickup circuit. In both cases, the sensors are non-intrusive and clamped around high-voltage cables between the spark plug and ignition coil or magneto [9]. This method is less reliable because typically only the signal of one spark plug is used and if the firing voltage for some reason is not generated (in the corresponding wire) while the engine is working, the counter will not be incremented. The main disadvantage, however, results from its application, which is confined to petrol engines only.

The third type uses vibration's analysis. This method uses a simple fixed threshold, or some other algorithm, to detect the engine's state. It is non-intrusive, and the installation process is simple. In order to obtain accurate results the counter should be installed as close as possible to the engine. An hour meter of this type is compatible with any engine, and it can be used with any other kind of machinery, that produces vibrations. The only challenge could be the accuracy of the detection. Commercial solutions based on this solution are already available [10]. The solution shown in figure 1 constitutes a tiny device with a minimum current consumption of 6 µa, which allow achieving an autonomy of 2.5 years with a CR2032 battery. The device allows the selection of two levels of sensitivity. This hour meter provides useful information, but it requires a periodical reading of the information shown on display. This supervisory task, however, can be automated.

Fig. 1. Hour meter with vibration based working principle.

2.2 FAULT DETECTION IN IC ENGINES

2.2.1 MONITORING METHOD

Predictive detection strategy in engines can use different monitoring methods, namely: vibration analysis, oil analysis, performance analysis, thermography, or ferrography analysis. Among them, vibration analysis is a particularly interesting technique because it not only enables a non-intrusive monitoring but also the identification/classification of faults. It can also be used to support periodic and constant monitoring of engines.

Vibration analysis has about 60 years of history [11]. Originally, this type of analysis was mostly used in potentially dangerous industries like petrochemical and nuclear where machinery condition is critical. The series of unfortunate accidents in these industries during several decades and its significant economic consequences gave rise to the growth of this type of analysis [12]. Subsequent evolution of piezoelectric material and advances of microprocessors and microelectromechanical systems (MEMS) made this analysis one of the most common in the area of machine condition monitoring.

An early example of vibration analysis for fault detection in IC engines can be found in a mechanic's stethoscope (see Fig. 2).

Fig. 2: Mechanic's stethoscope.

This tool allows the detection of different problems, including worn bearing and blocked injector. Thus, the automation of this process can improve reliability and bring the ability to detect more complex issues.

2.2.2 VIBRATION SENSING

Vibrations are characterized by their displacement, velocity, and acceleration. Non-intrusive sensors are used to obtain each of these characteristics. However, in the case of displacement, existing sensors can only measure relative values [1]. Moreover, the nature of mechanical systems is such that appreciable displacements only occur at low frequencies, therefore in the general study of mechanical vibration, displacement measurements are of limited value [13].

There are two types of acceleration transducers or accelerometers: piezoelectric and MEMS. MEMS-based accelerometers are cheap and have a digital interface but have a cutoff frequency of nearly 1 kHz, or less, whereas piezoelectric accelerometers are expensive and have wider bandwidths (generally about 10 kHz).

The price and performance of velocity transducers are close to the piezoelectric accelerometers. However, their typical frequency limit is only of a few kHz. Apart from higher frequency ranges, a piezoelectric accelerometer has a higher dynamic range and does not have internal moving parts [9].

PVDF piezo films constitute another option. They combine acceptable prices with a wide scale of bandwidth measurements. They, however, are very sensitive to Electromagnetic Interference (EMI) and require protection in harsh environments.

2.2.3 SIGNAL PROCESSING

In the case of IC engines, regardless of the type of sensor used to capture vibrations, the signal is non-stationary and multicomponent. Due to the number of components that compose the signal, time domain analysis is complicated. Some components can change their amplitude or frequency over time, and these variations are a primary source of information about the engine condition. Frequency domain analysis tools like Fast Fourier Transform (FFT) show different components but do not indicate their changes. However, time-frequency (TF) analysis allows tracking variations on time and frequency domains simultaneously, and that is why it is commonly used in this area.

Several methods can be used for TF analysis, but the improvement of existing ones and the addition of new ones does not stop. Some works have been dedicated to describe and classify these existing methods [14][15][16]. According to [16], all methods can be classified into six groups: (1) linear TF representation, (2) bilinear TF distributions, (3) time-varying higher

order spectra, (4) TF Auto-Regressive Moving Average (ARMA) model, (5) adaptive parametric and (6) non-parametric TF analysis.

Despite the diversity of methods, the most used ones belong to linear TF representation and to the Cohen's class distributions, which are part of bilinear time distributions. In the following, these methods are described considering their original mathematical expressions expressed as a function of continuous signals.

2.2.3.1 Linear TF representation

The two main methods of the linear TF representation are Short-time Fourier transform (STFT) and the Wavelet transform.

2.2.3.1.1 Short-time Fourier transform

In the case of STFT, the signal is firstly divided into short segments, and a Fourier transform is afterward applied to each segment, giving a variation of the spectrum with time:

$$STFT_x(t,f,h) = \int_{-\infty}^{+\infty} x(u)h^*(u-t)e^{-j2\pi fu}\,du \qquad (1)$$

In this equation, t represents the time, f the frequency and h(t) is a short time analysis window.

The fixed window length does not allow obtaining the same resolution in the time domain for low-frequency and high-frequency components. Due to the Heisenberg-Gabor inequality, it is also not possible to obtain a fine resolution in the time domain and frequency domain simultaneously [17]. Due to these disadvantages, this method is rarely used. The only work that was found to use the STFT, applied it in the detection of faults in a jet engine [18]. On the other hand, STFT is sometimes used as a reference, i.e. to evaluate the performance of other methods, like for instance in [19].

2.2.3.1.2 Wavelet transform

The wavelet transform decomposes a signal into wavelets, in the form of functions obtained by dilations or translation of a prototype function called mother wavelet:

$$(Tf)(a,b) = |a|^{-1/2} \int dt f(t)\psi\left(\frac{t-1}{b}\right) \qquad (2)$$

In this equation, defined as Continuous Wavelet Transform (CWT), a represents a translation parameter and b a dilation parameter. Different mother wavelets $\psi(t)$ can be used. The following figure shows some of them (see Fig. 3).

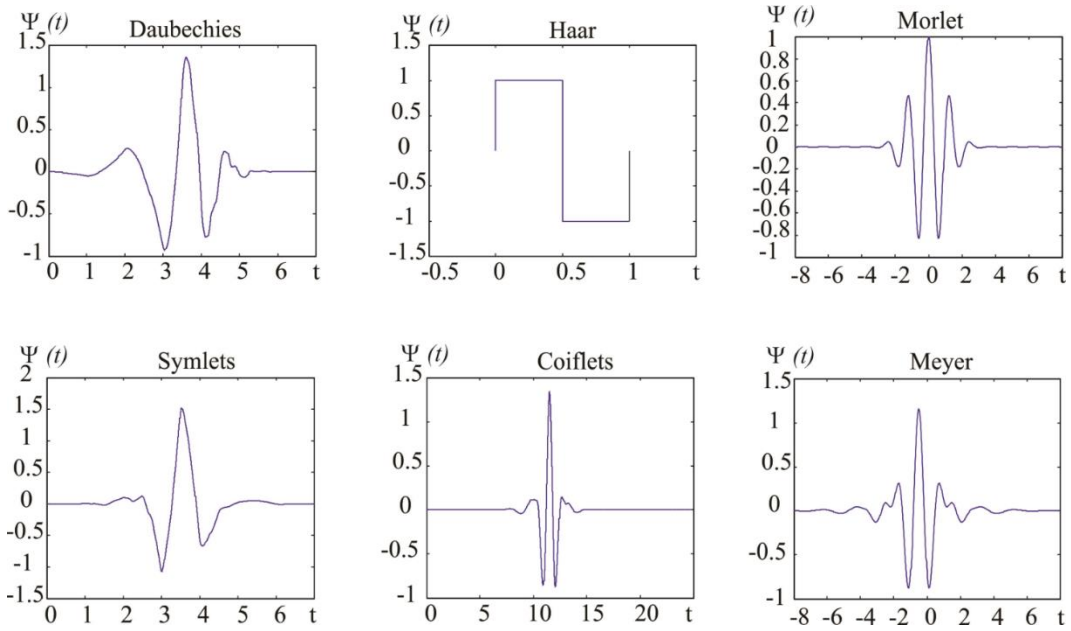

Fig. 3. Mother wavelets.

Unlike STFT, the window length of wavelet transform varies with the frequency, which allows maintaining the same resolution for low and high frequencies.

A discrete version or Discrete Wavelet Transform (DWT) is shown below:

$$T_{m,n}(f) = a_0^{-m/2} \int dt f(t) \psi(a_0^{-m} t - n b_0) \tag{3}$$

In this equation n represents the translation parameter, m is the dilation parameter and a_0 , b_0 vary according with the wavelet used.

Several works have successfully used a discrete wavelet transform to detect faults in IC engines. In [20] misfire detection using wavelet transforms have shown to be more effective than traditional methods. In [21] a Morlet wavelet was used for acoustic signal processing to provide information about IC engine condition. The authors used four directional microphones, which were installed in different positions to capture a data, before applying a wavelet transform. According to the results, the fault detection accuracy rate depends strongly on a microphone's position, reaching an accuracy of nearly 80-90% for the best position. The work done in [22] illustrates the advantage of the wavelet analysis as a time-frequency method

when compared with the analysis in the frequency domain. In [23] and [24] successful use of DWT for fault detection in IC engines was done allowing a real-time monitoring.

In order to be able to compare the performance of the wavelet transform, with other TF methods, a scalogram is used. A scalogram is a method of visualization of the wavelet transform in the TF domain:

$$SC_x(t,a;h) = \int_{-\infty}^{+\infty}\int_{-\infty}^{+\infty} |T_x(t,a;\psi)|^2 dt \frac{da}{a^2} \tag{4}$$

The relation between wavelet transform and wavelet scalogram is similar to the relation between STFT and Fourier spectrogram.

2.2.3.2 Cohen's class distributions

The Fourier spectrogram, Wigner-Ville (WV) and derivatives of WV are Cohen's class distributions which include some parametrization function to remove or, at least, attenuate interference terms.

2.2.3.2.1 Fourier spectrogram

The Fourier spectrogram is a squared modulus of the STFT:

$$SP_x(t,v) = \left| \int_{-\infty}^{+\infty} x(u)h^*(u-t)e^{-j2\pi vu}\, du \right|^2 \tag{5}$$

It represents a spectral energy density, with a time-frequency resolution equal to the STFT.

In [25] the spectrogram was used to detect a broken rotor bar of an induction motor. In [26] the spectrogram was also used for fault detection in a wind turbine. Several distributions are compared in this later article, with the spectrogram showing a good readability, but also the lowest time-frequency resolution.

2.2.3.2.2 Wigner-Ville distribution

The Wigner-Ville distribution (WVD) is a key distribution of Cohen's class, expressed by:

$$\begin{aligned} WV_x(t,f) &= \int_{-\infty}^{+\infty} x\left(t+\frac{\tau}{2}\right) x^*\left(t-\frac{\tau}{2}\right) e^{-j2\pi f\tau} d\tau = \\ &= \int_{-\infty}^{+\infty}\int_{-\infty}^{+\infty} A_x(\tau,v) e^{-j2\pi(vt+f\tau)} dv d\tau \end{aligned} \tag{6}$$

where $A_x(\tau,v)$ translates the ambiguity function:

$$A_x(\tau, v) = \frac{1}{2\pi}\int_{-\infty}^{+\infty} x\left(t+\frac{\tau}{2}\right)x^*\left(t-\frac{\tau}{2}\right)e^{-j2\pi vt}dt \quad (7)$$

WVD has a good TF resolution, but by being a bilinear function, suffers from cross-terms. In the simplest case, two signal components contribute to an interference term which is located in the middle point between signal components. The interference term has an oscillating nature, and its oscillation frequency is proportional to the distance between signal components. Thus, readability decreases with the increase of signal components.

In [27] the WVD was used for fault detection in mechanical reducer gearset, reaching a high recognition rate. In [28] this method was used for fault detection in power transformers. WVD was also used for IC engine fault diagnosis [29][30]. Results showed a high diagnostic accuracy. In [29] vibration acceleration was used for diesel engine condition monitoring whereas in [30] acoustic signal was used for scooter's engine condition monitoring.

One of the ways to reduce cross-terms is to use some parametrization function $f(\tau, v)$ to provide smoothing. There is a considerable number of distributions that use some parametrization functions and one drawback is common to all: smoothing is done at cost of time-frequency resolution.

In this field, the pseudo-WVD (PWVD) uses a window to attenuate interference terms:

$$PWV_x(t,f) = \int_{-\infty}^{+\infty} h(\tau)x\left(t+\frac{\tau}{2}\right)x^*\left(t-\frac{\tau}{2}\right)e^{-j2\pi f\tau}d\tau \quad (8)$$

The smoothed-pseudo WVD (SPWVD) typically allow achieving better suppression of interference terms:

$$SPWV_x(t,f) = \int_{-\infty}^{+\infty} h(\tau)\int_{-\infty}^{+\infty} g(s-t)\,x\left(s+\frac{\tau}{2}\right)x^*\left(s-\frac{\tau}{2}\right)e^{-j2\pi f\tau}d\tau \quad (9)$$

In [31] and [32] WVD, PWVD, and SPWVD were used for detecting rotor faults. In both articles, the performance of these methods was compared and SPWVD, as well as PWVD, did provide effective suppressing of cross-terms.

Another member of the Cohen's class is the Rihaczek distribution:

$$R_x(t,f) = x(t)X^*(f)e^{-j2\pi ft} \quad (10)$$

This distribution returns complex values, and for some applications, real values are more suitable. For this reason, the Margenau-Hill distribution was developed, which corresponds to the real part of Rihaczek distribution:

$$MH_x(t,f) = Re\{x(t)X^*(f)e^{-j2\pi ft}\} = \\ = \int_{-\infty}^{+\infty} \frac{1}{2}\big(x(t+\tau)x^*(t) + x(t)x^*(t-\tau)\big)e^{-j2\pi f\tau}d\tau \quad (11)$$

In [33] the Margenau-Hill distribution was used for evaluating arterial elasticity. According to the authors, this method was able of obtaining a notable difference between healthy volunteers and patients with the already diagnosed cardiovascular disease.

For better cross-terms rejection a pseudo-Margenau-Hill distribution was developed:

$$PMH_x(t,f) = \int_{-\infty}^{+\infty} \frac{h(\tau)}{2}\big(x(t+\tau)x^*(t) + x(t)x^*(t-\tau)\big)e^{-j2\pi f\tau}d\tau \quad (12)$$

In [34] this distribution was used for damage detection in bimetal composite pipes and was able to identify them.

There is also the Margenau-Hill spectrogram:

$$MHS_x(t,f) = Re\{K_{gh}^{-1}F_x(t,f;g)F_x^*(t,f;h)\} \quad (13)$$

where $K_{gh} = \int h(u)g^*(u)du$, and $F_x(t,f;g)$ is the STFR of *x* (analysis window *g*).

In [35] this method was used to obtain a TF resolution similar to the Fourier spectrogram.

The next distributions belong to the group of reduced interference, which is a part of the Cohen's class.

2.2.3.2.3 Choi-Williams distribution

Choi-Williams distribution is one of these distributions:

$$CW_x(t,f) = 2\int\int_{-\infty}^{+\infty} \frac{\sqrt{\sigma}}{4\sqrt{\pi}|\tau|}e^{-f^2\sigma/(16\tau^2)}x\left(t+f+\frac{\tau}{2}\right)x^*\left(t+f-\frac{\tau}{2}\right)e^{-j2\pi f\tau}df\,d\tau \quad (14)$$

This distribution was used in cardiovascular diseases detection [36][37] and in the study of gearbox prognosis [38]. In [39] this method was also used for chirping mode signals visualization in Tokamak plasmas, and Choi-Williams distribution provided better TF resolution comparing to Fourier spectrogram.

2.2.3.2.4 Born-Jordan distribution

The Born-Jordan distribution also belongs to the reduced interference distribution group:

$$BJ_x(t,f) = \int_{-\infty}^{+\infty} \frac{1}{|\tau|}\int_{t-|\tau|/2}^{t+|\tau|/2} x\left(s+\frac{\tau}{2}\right)x^*\left(s-\frac{\tau}{2}\right)ds\,e^{-j2\pi f\tau}d\tau \quad (15)$$

It was used in the medicine area for electrocardiogram analysis [40] and electromyographic signal [41]. In [41] it showed a TF resolution similar to the Choi-Williams or Cone-Shaped Kernel distributions, better than the Fourier spectrogram or scalogram. Also, it showed fewer cross-terms, when compared with the WVD method.

2.2.3.2.5 Zhao-Atlas-Marks distribution

Zhao-Atlas-Marks distribution (ZAMD) or Cone-Shaped Kernel distribution is another member of the reduced interference distribution group:

$$ZAM_x(t,f) = \int_{-\infty}^{+\infty} \left[h(\tau) \int_{t-|\tau|/2}^{t+|\tau|/2} x\left(s+\frac{\tau}{2}\right) x^*\left(s-\frac{\tau}{2}\right) ds \right] e^{-j2\pi f\tau} d\tau \quad (16)$$

In [42] it was used for stator short circuits detection in permanent magnet synchronous motors. In [43] this distribution was also used for broken rotor detection through vibration analysis. In [44] different TF distributions were compared including WV, Choi-Williams, Born-Jordan, and ZAMD. Up to a certain noise level, the last three distributions effectively reduce cross-terms. Among the three methods, the ZAMD also needed less computational time. In [45] ZAMD and other distributions were tested in the detection of rotor faults in brushless DC motors. According to the authors' conclusions, ZAMD provided high cross-term suppression, but Choi-Williams offers a better compromise between TF resolution and cross-term suppression.

2.2.3.3 Evaluation of the methods

While the above methods can be used to generate TF representations of the measured signals, this by itself do not allow the detection of faults. In order to detect faults, they need to be complemented with other methods. Several methods can be used to assess and compare these TF representations. In the following, three main methods are described: visual analysis, Rényi entropy and pattern recognition accuracy [46].

2.2.3.3.1 Visual analysis

Visual analysis was used in most of the references shown in the previous chapter. This method is very popular because it allows performance comparison of different methods based on various properties, including the TF resolution, cross-terms presence, the number of components and its dynamic change. It, however, relies on human assessment and a person engaged in the processing of results must have certain skills and experience to achieve a

correct interpretation of the results. Even so, some subjectivity sometimes takes place. Thus, automatic methods should be considered like the ones that we will describe in the following.

2.2.3.3.2 Renyi Entropy

The Rényi entropy (for the discrete outputs) is defined as:

$$R_x^{\alpha} = \frac{1}{1-\alpha} log_b \left(\sum_n \sum_k \left(\frac{TF(n,k)}{\sum_n \sum_k |TF(n,k)|} \right)^{\alpha} \right) \quad (17)$$

where α represents the entropy order.

In [47] this method showed to be a promising method for TF information content measure.

2.2.3.3.3 Pattern recognition

A different approach is to perform the comparison of methods based on the accuracy of the pattern recognition. This is a popular method. It consists in the classification of extracted features. The feature extraction is the essential part of the process of fault detection, and it strongly influences the recognition accuracy. This method is used in some of the works referenced in the last chapter, as for instance in [27] and [28].

In [46] a direct correlation between Rényi entropy and pattern recognition was also found.

2.3 COMMUNICATION SOLUTIONS

In the process of fault detection, the data obtained from the engine needs to be transmitted to a server on the Internet. At this level, several solutions can be used. By adding wireless connectivity to hour meters, client devices/applications can periodically request the readings, informing users about the required maintenance procedure. Also, besides the total number of working hours, the corresponding working intervals can be collected for statistical analysis.

A smartphone, tablet or smartwatch are considered as a possible client device in this work. These devices have different wireless interfaces, which can be used to communicate with the hour meter. The infrared port is one of the oldest mobile phone interfaces. It uses the infrared region of the electromagnetic spectrum and requires a direct line of sight. Because of this limitation, this interface is rarely used. The standardization was provided by the Infrared Data Association (IrDA) group [48], but there are many devices with proprietary protocols. Nowadays, this interface is mainly used for the control of home appliances.

Near-field communication (NFC) is a short-range communication that uses electromagnetic induction. It operates on 13.56 MHz frequency at a typical working distance of about 4 cm, with speed rates of 106, 212 or 424 kbit/s [49]. It is mostly used in payments, file sharing or as a pairing method for Bluetooth low energy.

Bluetooth is another short-range wireless technology. It includes several versions or specifications, all within the same operation frequency – 2.4 GHz. The most common versions are the 2.1 and 4.x [50]. Version 2.1 supports Basic Rate (BR) mode – 1 Mbps and Enhanced Data Rate (EDR) mode 2 Mbps. It is mostly used for constant connections as with a mouse, a keyboard, a headset or as a cable replacement. Version 4.x is also known as Low Energy (LE). It is focused on power saving, and its maximum data rate is 1Mbps. The low power version has many applications as home automation, fitness metering, and beacons. These two versions are incompatible, and their data rates cannot be compared directly.

The Wi-Fi technology, different from the previous ones, can transport Internet Protocol (IP) packets, and thus provide direct access to the Internet [51]. It operates on a frequency level of 2.4 or 5 GHz and includes four standards: a, b, g, n. Wi-Fi is typically used to provide wireless access to the Internet, and so it truly embraces the IoT logic. However, its power consumption is much higher than the Bluetooth or NFC interfaces.

At the higher layers different solutions can be used to communicate between the mobile terminal and the server that processes data like Constrained Application Protocol (CoAP) [52], or Message Queuing Telemetry Transport (MQTT) [53], in addition to WebAPIs RESTful based on Hypertext Transfer Protocol (HTTP), for communication with IP servers using JSON ou XML. As for communication with the sensors, the MQTT is one of the protocols that has gained more scope.

Since the aim of this project is to automate the hour metering process, the infrared interfacing and NFC were not considered as a viable solution due to their restricted range. Also, the Wi-Fi connection was considered as consuming too much to enable more than a year of autonomy. Among the several solutions, since the power consumption is a critical issue, the Bluetooth, especially the LE version, was considered to be better suited.

3. NON-INTRUSIVE MONITORING SYSTEM

This chapter presents the proposed solution for the non-intrusive monitoring system, and also the analysis for the selected components to be used.

3.1 PROPOSED SYSTEM ARCHITECTURE

As previously mentioned, this work proposes an IoT solution for a non-intrusive low-cost monitoring system to detect faults and register working hours of IC engines, focusing boat engines. Fig. 4 illustrates the proposed system. An IoT device is installed in a boat engine to collect engine's vibration data and send it to a user's smartphone via Bluetooth communication interface. The smartphone can pre-process this data and also send it to the internet, to a cloud-based server, where all the data is stored and continuously analyzed. The smartphone can also serve as a user interface with the system, which should include an app to allow the user to view all data results or be advised about the engine's maintenance procedures.

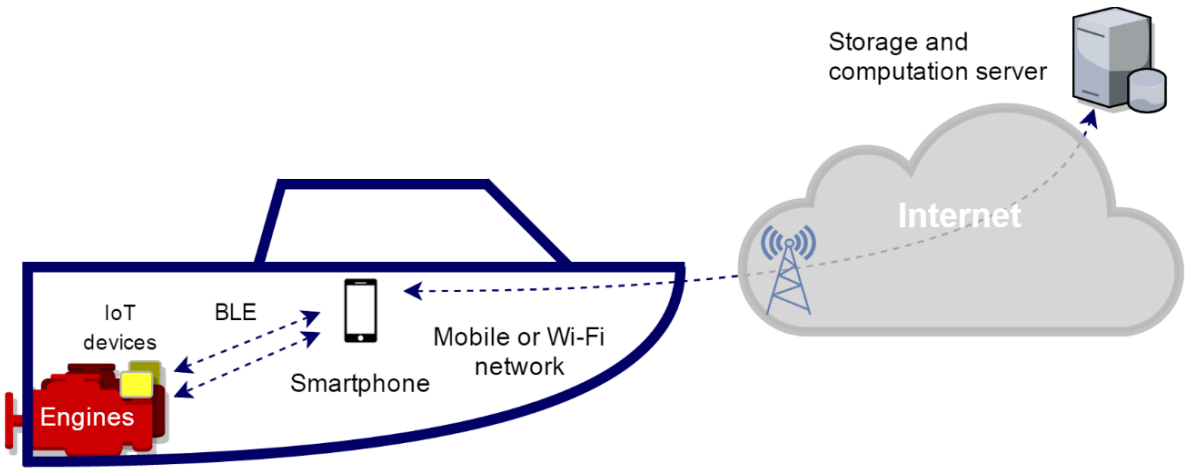

Fig. 4. System architecture

After the mounting of the device on the engine, the pairing procedure must be performed between the client device (user's smartphone) and the developed IoT device, establishing a

connection between these two devices. Following this procedure, a calibration routine should be executed for correct detection of the engine's state. Moreover, this calibration routine must be executed after each battery replacement, as the position in which the module was installed can be different and a reliable detection of the engine's state is not guaranteed without the calibration procedure. After the calibration, the IoT device starts the constant monitoring of the engine state, in order to track working hours and for the BLE module to start its advertising routine each time the engine is started. During an advertising period, a client device can connect to the IoT device, it in order to retrieve the information using a software application. This user's app, after being connected to the IoT device and after the motor starts running, initiates a periodical data monitoring routine on the vibration data, which is stopped if the client device is not within the motor's range.

A low power accelerometer will be used to monitor the engine's activity, and a piezoelectric polyvinylidene fluoride (PVDF) film is used to record the engine's vibration, for fault detection. Two devices are used because the system has to be low-power and allow faults to be identified. Therefore, the low-power accelerometer is used to be periodically activated and record the engine's working hours (providing a low-frequency rate vibration data signal). However, the piezoelectric sensor, which needs more power requirements due to the electronic circuit necessary to amplify and capture its data, will be activated sparsely in time to record a high rate vibration signal, to allow a fault detection analysis. In the next section, the component selection will be explained, providing more in-depth information on the sensors and system requirements.

As boats can have more than one engine, different implemented IoT devices are installed in every boat's engines to capture the vibration's information, which will then be sent to a smartphone or another client device using a Bluetooth Low Energy (BLE) interface. Each device has a distinct ID. After receiving the data, the client device forwards it through a Wi-Fi or mobile network connection to a cloud server on the Internet, for further processing. This is done using a Web Application Programming Interface (API) where the device's ID acts as a unique key. The server then processes the received data, notifying the client's terminal in case it detects any fault. It also increments the number of hours that the engine has been working, making this information available to the mobile terminal and notifying the user in case a routine maintenance is needed. Besides processing it, the server also stores the data for statistical purposes, i.e. the user can access historical data about the engine(s) usage. The client's mobile device and application simultaneously act as an Internet gateway of Machine-to-Machine Communications (M2M) and Human-Machine Interface (HMI).

The developed technique for fault detection includes data acquisition, analog and digital pre-processing and digital processing. The most important part of the digital processing, in this case, is a Time-Frequency Analysis (TFA). Several TFA algorithms are tested with real data to select the best solution to detect faults in such engines.

3.2 SENSORS AND COMPONENTS SELECTION FOR THE IOT DEVICE

This section begins with a more detailed definition of the requirements and key characteristics. After that, based on these requirements, the architecture of the IoT device is defined, and for each block the required components are selected. The selection of components is done according with the characteristics which are considered relevant for the corresponding module, and considering that this is a first prototype intended to make a proof-of-concept.

3.2.1 KEY CHARACTERISTICS

The main requirements imposed to the IoT device are low price, small size, two years autonomy and a wireless connectivity by Bluetooth.

One example a device that corresponds to these requirements is the SensorTag kit CC2650STK from Texas Instruments (TI) [54]. It is a reference design built around CC2650 wireless microcontroller unit (MCU) which includes an ARM Cortex-M3 microprocessor and a series of peripherals. There are few remarkable features like autonomous sensor controller, support for different protocols (BLE, ZigBee, 6LoWPAN, and ZigBee RF4CE) and ultra-low power (1 µA in a standby mode and 100 nA in a shutdown mode). Apart from MCU, this kit comprises a number of sensors which allow to measure ambient or object temperature, the intensity of light, humidity, absolute barometric pressure. It also has an accelerometer, gyroscope, compass, digital microphone and reed sensor. Next table resumes characteristics of the kit which are essential for this work (see Tab. 1).

Tab. 1. CC2650STK characteristics.

Price	**$29**
Battery type	Coin cell (CR 2032)
Range	50 m
Battery lifetime	One year (1-second report interval)
Size (W x H x D)	5 x 6.7 x 1.4 cm

These characteristics will be used as a reference during development. Usage scenario also imposes several requirements. The sensing of the working periods is done by a constant monitoring of the engine's state. The Bluetooth connectivity on the IoT device is switched on when the engine starts. This allows the update of the information on a client's device only when the engine is working. In addition to it, a client device can initialize the engine's condition check procedure.

Vibration analysis can be used to check both, the on/off state of the engines and its condition. However, the identification of the on/off state imposes a much lower power consumption of the hardware, which is partially compensated by lower performance needs. Thus, it can operate continuously due to the fact that it consumes little.

In the case of the condition monitoring, the sensitivity of the sensor is more important than the power consumption - because this check is only occasionally done. It is then difficult to implement a system that meets both requirements while assuring low hardware costs. In order to do it, a distinct hardware block for each of these tasks is used. A time counting block is required to provide the information about current time. Also, the information about working hours should be retained when the power goes down which implying the integration of a non-volatile memory, to save this information. A Bluetooth module is also needed for communication purposes, and also a control block, to implement all the control procedures and interface with other peripheral blocks.

3.2.2 ARCHITECTURE OF THE IOT DEVICE

The architecture that results from the requirements described in the previous subsection is shown in figure 5.

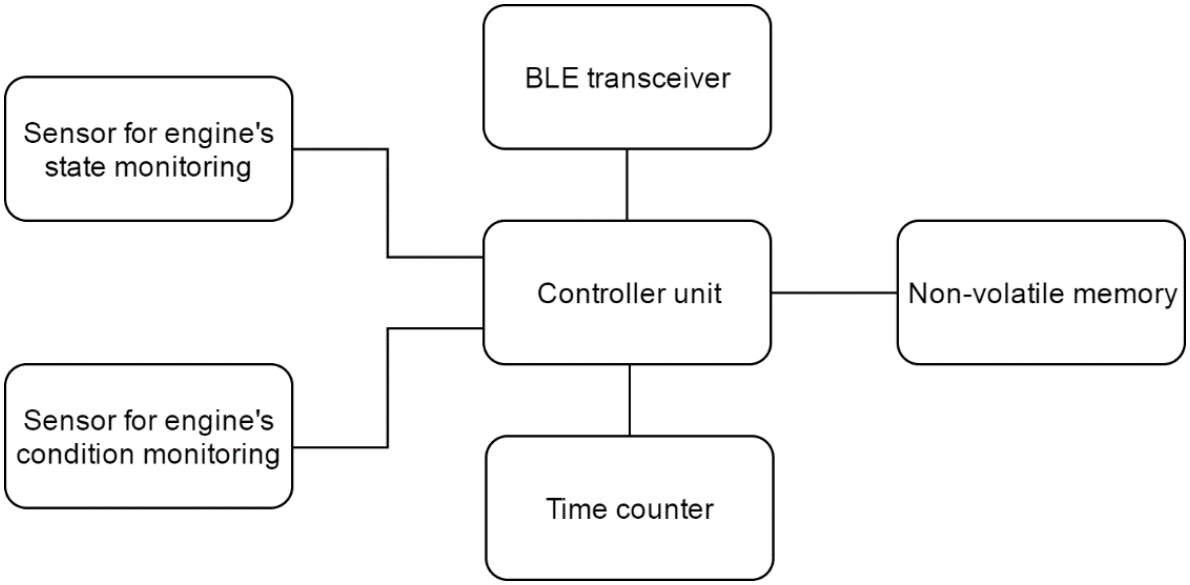

Fig. 5. Device architecture.

After the study of the market, it was concluded that for the Bluetooth transceiver and controller unit an MCU that incorporate a Radio Frequency (RF) Transceiver and a microcontroller would be the best solution because they usually have low power consumptions and high levels of integration. Furthermore, there are pre-certified modules that apart from the mentioned MCU include all the necessary analog circuitry for the RF. Another advantage is the minimal number of external components.

As for the non-volatile memory, there are four principal types: Electrically Erasable Programmable Read-Only Memory (EEPROM), flash memory, Non-Volatile Random-Access Memory (NVRAM), and Ferroelectric Random-Access Memory (F-Ram).

The timer of the MCU can be used as a time counter. However, for saving working intervals, the knowledge about current time/date is required. For this purpose, Real-Time Clocks (RTC) are typically used.

MEMS accelerometers are better suited for engine’s state monitoring whereas PVDF films are a better choice for condition monitoring. Still, the PVDF films needs a signal conditioning circuit.

The system architecture was modified taking into consideration the described solutions. It is shown in figure 6.

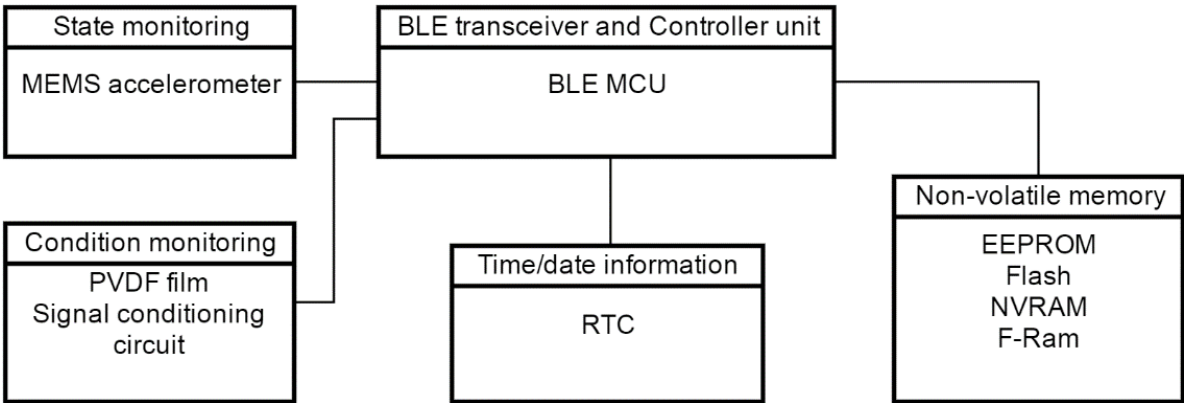

Fig. 6. Modified system architecture.

3.2.3 MEMS ACCELEROMETER

After analyzing the solution available in the market, two candidates were selected for a more detailed comparison. Their characteristics are summarized in the following table (Table 2).

The IIS328DQ [55] provides wider temperature range and output data rate (ODR), when compared with the ADXL362 [56]. It also supports an Inter-Integrated Circuit (I2C) interface, in addition to a Serial Peripheral Interface (SPI), and comprises a programmable high-pass filter. The high-pass filter can be used to remove static acceleration. The cost of the ADXL362 is twice the cost of the IIS328DQ. However, its current consumption is far lower than the one of the IIS328DQ or any other accelerometer available in the market. The ADXL362 provides additional features, like autonomous interrupt processing, standalone sleep/wake transition and embedded FIFO. These features allow the reduction of the number of communications between the MCU and the accelerometer and thus, the current consumption.

Given these advantages, we opted to use the ADXL362, despite the difficult of assembly it imposes and its significantly higher price.

Tab. 2. Characteristics of chosen MEMS accelerometers.

Characteristic	*IIS328DQ*	*ADXL362*
Price for 1000 pieces	€ 2.20	€ 4.86
Supply voltage range	2.16 – 3.6 V	1.6 – 3.5 V
Temperature range	-40 ˚C to +105 ˚C	-40 ˚C to +85 ˚C
Resolution	12 bits	12 bits
Measurement range	±2g/±4g/±8g	±2g/±4g/±8g
Output data rate	50, 100, 400, 1000 Hz	12.5, 25, 50, 100, 200, 400 Hz
Interface	SPI/I2C	SPI
Interrupt	2	2
Current consumption modes at 3.3 V voltage supply	Normal: 250 µA Low-power: 10 µA Power-down: 1 µA	Ultralow noise: 15 µA Low noise: 4.5 µA Normal: 2.7 µA Wake-Up: 270 nA Standby: 10 nA
Extra features	Programmable high-pass filter	Autonomous interrupt processing, standalone sleep/wake transition, embedded FIFO, on-chip temperature sensor
Soldering	++	+

3.2.4 PVDF FILM

Only one suitable PVDF film sensor was found. It is a rectangular element of piezo film with silver ink screen printed electrodes [57]. Its operating temperature ranges from -40 to 60 °C. There are two versions with or without lead wires attached. Different film dimensions are available. The film without leads can be fixed using double-sided tape or epoxy, providing direct attachment to the PCB. The sensor is also low-cost – version without leads costs € 2.38 for 1000 pieces. There isn't any information about frequency response, however, in the datasheet of a similar film of the same manufacturer [58] a frequency response chart is shown (see Fig. 7).

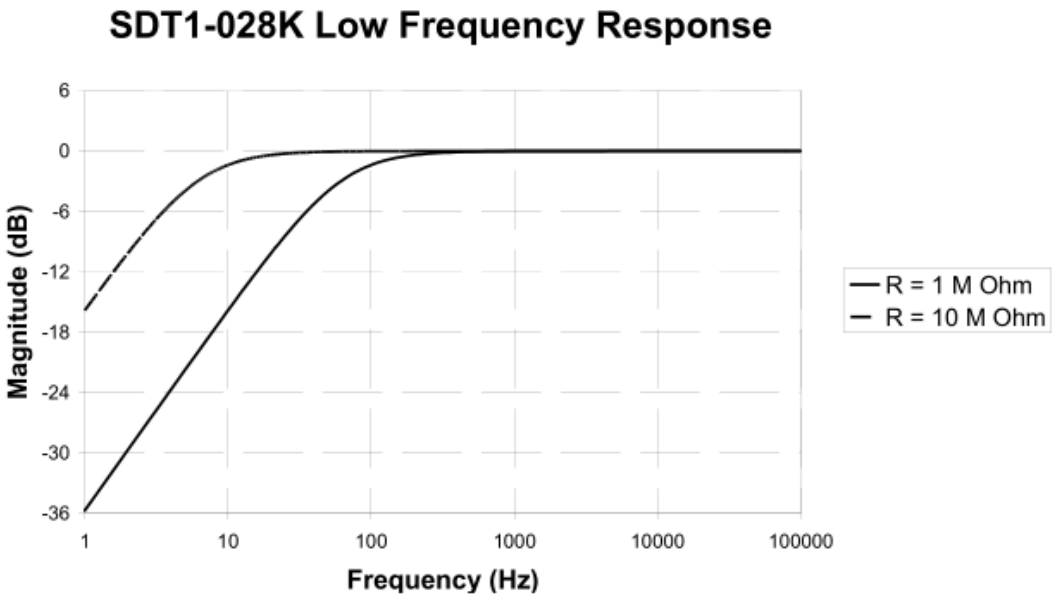

Fig. 7. PDVF film sensor frequency response, obtained from [58]

The transfer characteristic of the film is similar to the frequency response of a high-pass filter, and its cut-off frequency depends on the input impedance of the connected circuit. It can be seen that the curve is flat up to 10 MHz. This film is folded over on itself providing shielding and coaxial cable attached to the sensor. Both films are shown in figure 8.

The shielded version with coaxial cable is better suited for tests because the hardware can be changed independently, but also since the shield protects against EMI [59].

Fig. 8. PVDF film sensors: version without leads on the left and shielded version with coaxial cable on the right.

3.2.5 RTC

Among the huge number of components in the market, there is one that stands out for its extremely low current consumption and reasonable price. The AB18X5 [60] from Abracon has a minimum current consumption of 14 nA if an integrated RC oscillator is used and costs

€0.854 when 1000 pieces are bought. Current consumption in other two modes is also very low: 55 nA with an external crystal oscillator and 22 nA when an internal RC oscillator is used (and periodical autocalibration is performed using external crystal oscillator as a reference). Despite its low consumption, this component not only provides basic timekeeping functions but also: (1) allows the definition of alarms, (2) generates output clock or reset signal, and (3) controls external components using integrated power switch which can be controlled manually or by interruption signal. Interruption signal generation is also available as well as a watchdog timer. A 256 bytes volatile RAM is also available. The availability of a communication interface depends on its version and can be I2C or SPI. It supports industrial temperature ranges. Its operating voltage ranges from 1.5 to 3.6 V. Hot air station can be used for soldering when using the QFN-16 package.

3.2.6 NON-VOLATILE MEMORY

Before analyzing the components available in the market, we started by defining the required size of the memory. The non-volatile memory, like already was mentioned, is required to hold the total working time and working intervals in the future. It also can be used to store calibration data or other information. Considering that the accumulated working time is expressed in seconds, a 32-bit unsigned integer seems to be an appropriate choice as it allows storing 4294967296 seconds, or 1193046 hours, which is about 136 years. Also, for each working interval, a start and stop time instants must be stored. The system should be capable of storing at least the last 100 working cycles. Start and stop instants can be stored in the Unix time format, and thereby 32 bits are required for each instance or 64 bits for each working cycle. By reserving ten 32-bit numbers for future use, the minimum size of the memory will be $32 + 64 \times 100 + 32 \times 10 = 6752$ bits.

As was mentioned earlier, there are four main non-volatile memory types: EEPROM, flash, NVRAM, F-Ram. In each of these types of the memory a component was chosen, before performing a deeper comparison. Table 3 summarizes the relevant characteristics of the compared components.

Tab. 3. Non-volatile memory components comparison.

Characteristic	*MR25H128A*	*AT25SF041*	*M95160-DRE*	*FM24CL16B*
Memory type	MRAM	Flash	EEPROM	F-Ram
Price for 1000 pieces	€ 1.77	€ 0.223	€ 0.256	€ 1.01
Supply voltage range	2.7-3.6 V	2.5-3.6 V	1.7-5.5 V	2.7-3.65 V
Temperature range	-40 ˚C to +85 ˚C	-40 ˚C to +85 ˚C	-40 ˚C to +105 ˚C	-40 ˚C to +85 ˚C
Memory size	128 kbit	4 Mbit	16 kbit	16 kbit
Endurance	Unlimited	100k Program/Erase Cycles	4kk write cycles at 25 °C; 1.2kk; write cycles at 85 °C; 900k write cycles at 105 °C	100 trillion read/writes
Data retention time	20 years	20 years	More than 50 years at 105 °C; 200 years at 55 °C	More than ten years at 85 °C; 38 years at 75 °C; 151 years at 65°C
Interface	SPI	SPI	SPI	SPI/I2C
Current consumption modes	Active Read: 3 mA @ 1 MHz Active write: 13 mA @ 1 MHz Standby: 115 µA Sleep: 30 µA	Erase or program: 16 mA Read: 6 mA @ 20 MHz Standby: 25 µA Deep power-down: 5 µA	Read: 5 mA @ 20 MHz Write: 2 mA Standby: 3 µA @ 20 MHz	Average current for SPI: 0.2 mA @ 1 MHz; 3 mA @ 20 MHz Average current for I2C: 300 µA @ 400 kHz; 100 µA @ 100 kHz Standby: 6 µA
Ease of use	+++	+	++	+++
Extra features	No write delays	Supports Dual and Quad Output Read	-	No write delays
Soldering	++	+++	+++	+++

The MR25H128A [61] from Everspin Technologies is a magnetoresistive random access memory (MRAM), and it belongs to NVRAM type. Only this memory provides unlimited number of read/write operations, although, it is the most expensive one. Also, there is no delay between the write operations, and the communication protocol is simple. Current consumption in standby and sleeping mode is however high, when compared with the other alternatives.

The AT25SF041 [62] from Adesto Technologies is a flash memory. While being the cheapest one, it has the largest amount of memory and maximum operating frequency, when compared with the other devices. In addition to a slave output pin, data can be transferred to the master device using other pins which allow an increase of the data transfer rate. However, the number of program/erase cycles is limited to 100000. It is not possible to erase a single byte of the data, instead the whole page should be erased.

The M95160-DRE [63] from STMicroelectronics is an EEPROM memory. Is supports wider supply voltage and temperature ranges, when compared with the others. The number of read operations is unlimited, and the number of write operations is at least ten times bigger than of the flash memory.

The FM24CL16B [64] from Cypress Semiconductor is an F-Ram memory. The others the number of read operation is limited, however, the number of write/read operation is huge - 10^{14}. The supported communication interfaces depend on the version and can be SPI or I2C. Like the MRAM memory, it does not introduce a delay between write operations and the communication protocol is simple.

While all the compared components have sufficient memory size and data retention times, the F-Ram memory seems to be a more balanced solution that combines: high endurance, low current consumption, easy to use and I2C interface. Thus, we opted to selected it.

3.2.7 BLE MCU MODULE

In terms of Bluetooth, despite the variety of solutions on the market, there are three main modules that meet the imposed requirements: CC2650MODA from TI [65], BL652 from Laird [66], and CYBLE-212019-00 from Cypress Semiconductor [67]. The characteristics of the chosen modules are summarized in table 4.

The first module is based on the already mentioned CC2650. No external components are in this case needed. It includes I2C, SPI, and a 12-Bit ADC with a maximum sampling rate of 200 ksamples/s. Code Composer Studio from TI can be used as it is an Integrated Development

Tab. 4. BLE MCU modules comparison.

Characteristic	*CC2650MODA*	*BL652*	*CYBLE-212019-00*
Price for 1000 pieces	€ 6.87	€ 7.03	€ 6.44
Price of debugging probe	€ 15.63	€ 60.36	€ 9.40
Size	16.9 mm x 11 mm x 2.69 mm	14 mm x 10 mm x 2.1 mm	14.52 mm × 19.20 mm x 2.00 mm
BLE version	4.2	4.2	4.1
Operating temperature	-40 ˚C to +85 ˚C	-40 ˚C to +85 ˚C	-40 ˚C to +85 ˚C
Microcontroller	ARM Cortex - M3	ARM Cortex - M4 with floating-point unit	CYBL10XX7X
Max. operating frequency	48 MHz	64 MHz	48 MHz
DMIPS/MHz	1,2	n/a	0,9
EEMBC CoreMark® Score	142	215	n/a
Flash memory	128 kByte	256-512 kByte	256 kByte
RAM memory	8 kByte + 20 kByte	32-64 kByte	32 kByte
Max. TX output power	5	4	3
Voltage supply range	1.8 to 3.8 V	1.8 to 3.6V	1.9 to 5.5V
Low power modes	Idle: 550 µA Standby: 1 µA Shutdown: 150 nA	Standby: 1.2 µA Deep sleep: 400 nA	Deep sleep: 1.3 µA Hibernate: 150 nA Stop: 60 nA
I2C	+	+	+
SPI	+	+	+
ADC	12-bit, 200 ksps	12-bit, 200 ksps	12-bit, 1-Msps
DMA	+	+	-
Extra features	Ultra-Low-Power Sensor Controller	PPI, PMU	GUI for BLE config.
IDE w/o code limitation	+	+	+
Ease of program	+	++	+++
Number of ext. components	0	0	1-2
Soldering	+	++	+++
Compliance with Worldwide Radio Frequency Regulations	FCC, IC, ETSI, ARIB STD-T66, JATE	FCC, CE, IC, MIC	FCC, CE, IC, MIC, KC
BLE qualification	Declaration ID and QDID	Declaration ID and QDID	Declaration ID and QDID

Environment (IDE) and is free. The soldering is difficult because pads are exposed on the bottom side of module's PCB, and there are four ground pads that are distant from the edges of the board. Low-cost SimpleLink SensorTag Debugger DevPack or J-Link debug probe from Segger can be used, for program and debug purposes.

The BL652 module from Laird is based on a Nordic Semiconductor nRF52832 integrated circuit. It supports NFC, apart from BLE and like the previous module does not require external components. Peripherals include, among others, I2C, SPI, and 12-bit ADC with a sampling rate of 200 ksps. The current consumption is automatically optimized by a Power Management Unit (PMU) which detects the resources required by the different components in the system. Another interesting feature is the Programmable Peripheral Interconnect (PPI) which allows autonomous interaction between different peripherals, independent from the CPU. Laird recommends to use a smartBASIC, an event-driven programming language. It is designed to accelerate the software development process and provides high-level access to the BLE stack, peripherals, and non-volatile storage. However, debugging can be done only using print statements. As an alternative, it is possible to program in C using Nordic Software development kit (SDK) and the J-Link probe can be used for program and debug in this case. Nordic Semiconductor does not offer any IDE. The Embedded Studio can used. It is available for free for educational purposes. The soldering process is easy because of castellated solder pads.

CYBLE-212019-00 from Cypress Semiconductor is similar to the previous modules but needs one or two ferrite beads. It has two serial communication blocks, and each one can be used to implement an I2C or SPI interface. It integrates a 12-bit ADC with a sampling rate of 1 Msps. Cypress Semiconductor provides an easy-to-use and limitations-free PSoC Creator IDE. It allows to configure peripherals and BLE parameters using a graphical user interface (GUI). The MiniProg3 Program and Debug Kit or low-cost CY8CKIT-059 PSoC 5LP Prototyping Kit with Onboard Programmer and Debugger can be used to debug and program. Like in a previous module, castellated solder pads are used. Also, the spacing between pads is higher, therefore, the assembly process is easier.

All modules support industrial temperature ranges and have a number of certifications. The BL652 is the most powerful and compact solution. The CC2650MODA is in the second place in terms of performance, but the soldering and programming process is more difficult when compared with the others. The CYBLE-212019-00 has less processing power and is bigger than the others, but is the cheapest one. Its ADC sampling rate is five times higher compared to the other two modules which can be important for the engine's condition monitoring. The

product development process is facilitated due to the associated IDE and easy module assembly. As complex data processing will be performed on a client device, high performance is not required. Thus, we opted by selecting the CYBLE-212019-00 as a BLE MCU. It is shown in the following figure (see Fig. 9).

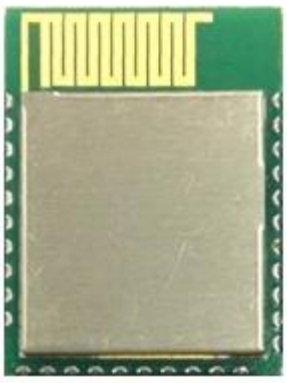

Fig. 9. CYBLE-212019-00 module.

4. PROTOTYPING

After selecting the necessary components, we proceeded to the device's implementation. Its description begins with the description of device schematic which is based on the modified device architecture shown in 3.2. In the following, we describe the implemented prototypes of the hour meter and condition monitoring blocks. In the case of the hour meter prototype, we explain the designed hardware and firmware. In the case of condition monitoring block prototype, the intermediate circuit design process is described, and some practical tests are performed to check its level of sensibility.

Fig. 10 shows the device's schematic based on modified system architecture.

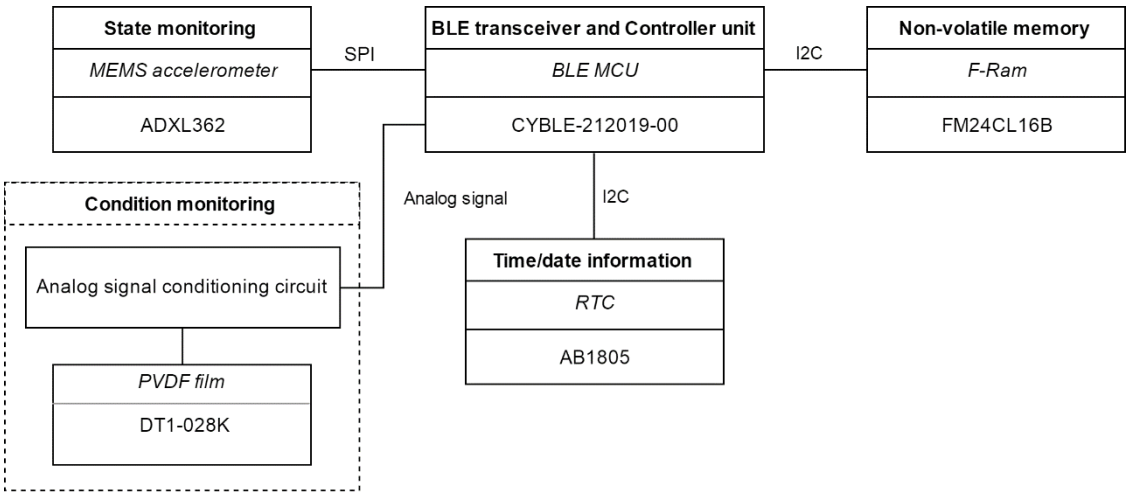

Fig. 10. Device schematic.

To save the space on the PCB, the I2C version of the RTC and F-Ram were used. Components for the analog signal conditioning circuit cannot be chosen without software simulation. All components are power supplied from the same source, hence, the voltage must be within 2.7-3.5V range. The minimum voltage is limited by the F-Ram and the maximum by the accelerometer. The circuit can be supplied from a single 3V lithium battery just like in the

case of Sensortag. However, batteries with bigger capacities like CR2450 or CR2477 can be used to increase the autonomy.

In order to implement the hour meter functionality, nearly all blocks are required, with the exception of the condition monitoring block which can be designed independently. Thus, two prototypes were constructed: one for hour metering and the other for condition monitoring. In the following, we describe each of these prototypes.

4.1 HOUR METER PROTOTYPE

4.1.1 HARDWARE

The following figure shows the layout of the hour meter prototype (see Fig. 11). In addition to the components depicted on the schematic (shown in Fig. 10), it includes a number of components required for the proper module operation. In terms of the size it is similar to the

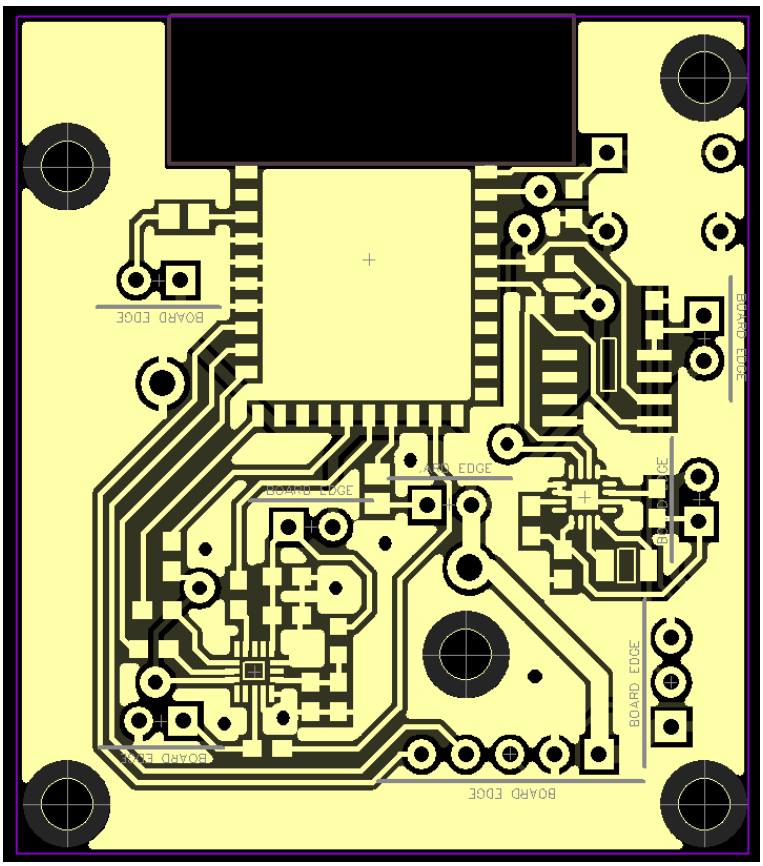

Fig. 11. Layout of the hour meter prototype.

Sensortag: 50 x 67 mm vs. 42x48 mm. It can be power supplied by an external source or 3V coin cell battery. Two vias are exposed for the battery holder, and several coin cell batteries are supported: CR2430, DL2430, CR2450, DL2450, CR2477. Program and debugging are done using dedicated pin header, and the current consumption of each key component can be measured using provided jumpers. A tactile switch is added to enable the reset of the MCU.

4.1.2 FIRMWARE

This chapter aims to describe the firmware implemented in the BLE MCU. At this moment, only the hour meter functionality is available.

The BLE service was created to enable information exchange and to be able to perform calibration, changing the device's setting. The structure of the service is shown in figure 12. The Log service is the primary service, and it is comprised of two characteristics: (1) Working time and (2) Calibration. The Working time characteristic consists of one field named Counter. It is a 32-bit unsigned integer which represents accumulated working hours. Set state is the associated descriptor with a one 8-bit unsigned integer field which is used to control the state of the counter (0x1 – the counter is on, 0x0 – the counter is off). Calibration is another characteristic which consists of the one field named Threshold. It is a 12-bit unsigned integer which is used to determine the engine state. The Update is the associated descriptor. It consists

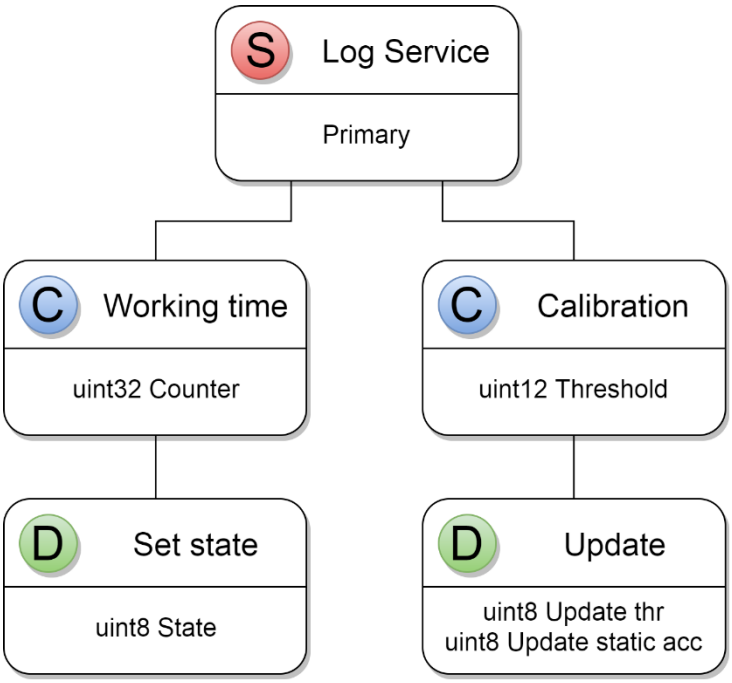

Fig. 12. Service structure.

of two 8-bit unsigned fields: (1) Update thr and (2) Update static acc. The first one is used to execute dynamic calibration and the second one is used to run the static calibration. To initiate calibration, the 0x6A must be written to the corresponding descriptor field. The purpose of the static calibration is to obtain a static acceleration of each axis of the accelerometer. Static acceleration depends only on the device position and not on the state of the engine. This calibration routine is performed when the engine is not running. The dynamic calibration is executed after the static calibration, to obtain the acceleration produced by the running engine. The output of this calibration is a threshold value which is calculated taking into account the results of the static calibration.

The firmware states and logic is shown in figure 13. Initially, the MCU is in the Start state, and it checks if it was switched off or was woken up from hibernation. In the first case, the initial configuration of RTC and accelerometer is performed, and the state changed to the BLE active. Thus, the calibration must be done after each switch off. In the second case, hardware configuration, counter state, and status of the accelerometer are verified. If (1) settings are not defaults, (2) the counter is on, and (3) activity event is detected by the accelerometer then the

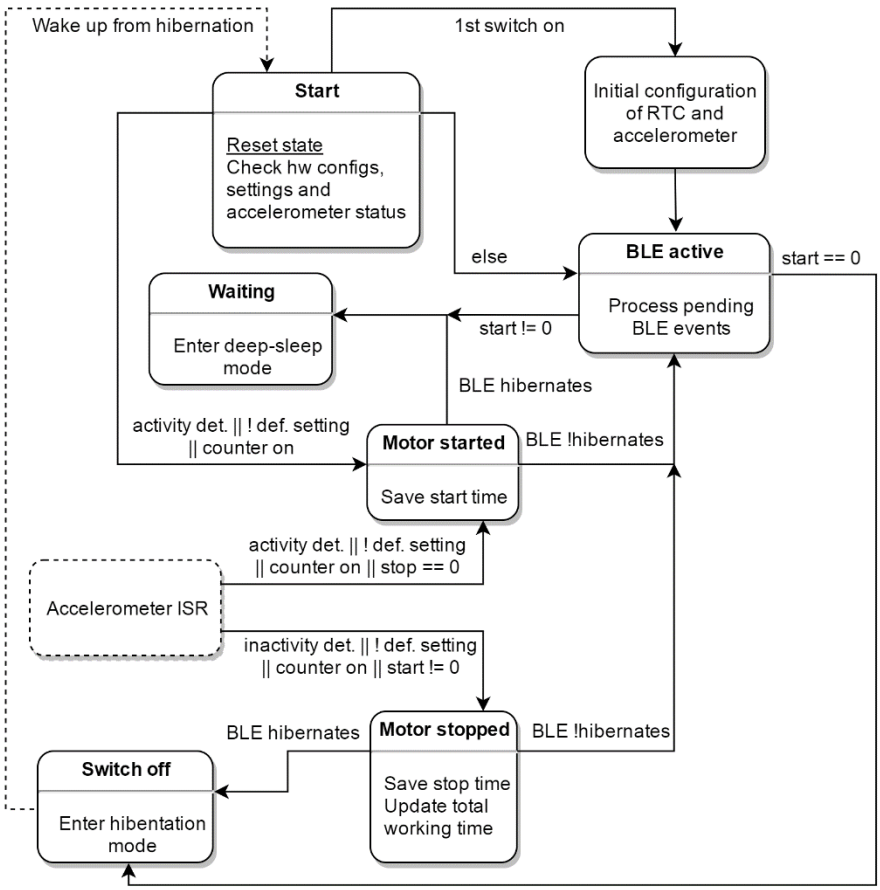

Fig. 13. Software states and logic.

state is changed to the Motor started. Otherwise, the state is changed to BLE active. In any case, before the transition to the other state, the BLE stack is initialized. In the Motor started state, the start time is saved into the volatile memory and if BLE part is not hibernated state is changed to the BLE active or in case it hibernated, to the Waiting state. In the BLE active state the advertising process is started, and the client device can establish a connection to read or write the data. It is 30 seconds long. In the case of connection event, the advertising is stopped. After disconnection, the advertising process is restarted. If a timeout occurs and the start time is non-zero (engine had started) the state changes to Waiting and MCU is put into the deep-sleep mode. Otherwise, the state changes to the Switch off, and the MCU hibernates. If the device was switched on and calibrations were not performed in the first advertising cycle, MCU switches off, and it will never wake up from hibernation because the activity/inactivity threshold is not configured. In this case, the reset button can be used to force the MCU to wake up and start the advertising process.

The activity/inactivity detection events are mapped to one of the accelerometer's interrupt output pins. In turn, this interrupt pin is connected to one of the MCU pins and thus a change of the engine's state generates an interrupt event in the MCU. The interrupt event causes the MCU to wake up both from deep sleep and hibernation. The Interrupt Service Routine (ISR) is executed in all states except the Switch off, as the MCU is reset after waking up from hibernation. The engine state is updated in the ISR only if the counter is on and settings are not default. Additionally, in the case of an activity detection event, the state is changed to Motor started, only if the stop time is equal to zero. As for inactivity detection event, the stage is changed to Motor stopped only if the start time is non-zero. With these two additional conditions, the consistency is guaranteed. In the Motor stopped state, the stop time is saved into volatile memory and the working time is calculated by subtracting the start time from the stop time. The total working time, which is saved in the non-volatile F-RAM memory, is updated then. Next, the state is changed to the BLE active if BLE part is not hibernated and to the Switch off state if hibernated.

In order to estimate the autonomy of the device, the average current consumption in different MCU states need to be measured. There are four possible MCU states: (i) deep sleep, (ii) hibernation, (iii) BLE advertising, (iv) BLE connection. The current consumption was measured only for first two states because in the other two states the consumption strongly depends on a number of parameters [68] which are adjusted during practical tests in the typical work environment (engine room in this case). The MCU is in deep sleep mode when the engine is working and the advertising period is expired. At the same time, the accelerometer is

working in a normal mode. Regarding the consumption of RTC and F-RAM memory, it does not depend on the state. The overall consumption of the device in this mode is approximately 11.5 µA. When the engine stops, the accelerometer automatically enters in low power mode, and its consumption decreases significantly. The MCU hibernates if there is no active connection or when the connection is over. The overall consumption of the device in this mode is approximately 6 µA.

4.2 PROTOTYPE OF THE CONDITION MONITORING BLOCK

The PVDF film cannot be directly connected to ADC of the MCU for several reasons. The input resistance of ADC of the chosen MCU is 2.2 kΩ. In this case, the lower cut-off frequency will be 26 kHz whereas the desirable value is approximately 20 Hz (which corresponds to 600 RPM in a four-cylinder engine). The ADC is unipolar, thus, it only accepts positive voltages. Finally, the amplitude of the captured signal may be low, requiring amplification. In order to meet these requirements, a signal conditioning circuit was designed. It consists of three stages. The first one is the input block and serves as a buffer, the second one amplifies the output signal of the first block, and the third one adds a DC offset.

Typically, the buffer circuit for piezo film sensors is implemented using junction gate field-effect transistor (JFET) or operational amplifier (op-amp). JFET is a simple solution and, generally, used as a unity gain buffer whereas op-amp is a more versatile solution as it can amplify the signal besides buffering. According to the TI's application report [69], two types of amplifier circuits are used: voltage mode or charge mode. The choice of the circuit type depends on the distance between the sensor and the circuit. A voltage mode amplifier is better suited when the sensor and the circuit are close to each other, otherwise, charge mode should be chosen. The voltage mode was chosen for this project because all the components are going to be mounted on the same Printed Circuit Board (PCB). The following figure shows the buffer stage with a voltage mode amplifier (see Fig. 14).

The Vin AC voltage source and C1 capacitor represent a piezoelectric simulation model. The transfer characteristic of the circuit is similar to a band-pass filter. The lower cut-off frequency is set by R8 resistor and the equivalent capacitance of the sensor as follows:

$$f_L = \frac{1}{2\pi \times R8 \times C1} \tag{18}$$

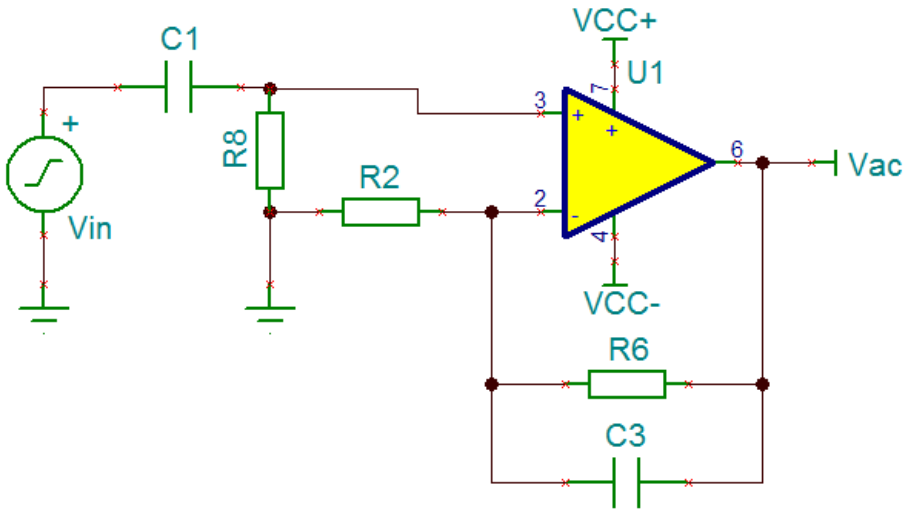

Fig. 14. Buffer stage of the conditioning circuit.

Where C1 is a fixed value specified in the datasheet of the sensor. Thus, the f_L can be adjusted only by variating R8. Its value is chosen in order to set the lower cut-off frequency to approximately 2 Hz. The higher cut-off frequency is set by R6 resistor and C3 capacitor as follows:

$$f_H = \frac{1}{2\pi \times R6 \times C3} \tag{19}$$

Both R6 and C3 can be adjusted, although, R6 influences on the gain of the circuit as shown below:

$$V_{ac} = \left(1 + \frac{R6}{R2}\right) V_{in} \tag{20}$$

Values of R6 and C3 are chosen in order to set the higher cut-off frequency to approximately 90 kHz. With the selected value of R2, the gain of this stage is equal to 5.09V/V or 14.13 dB. The AC transfer characteristic is depicted in the following image (see Fig. 15).

Inverting amplifier composes the second stage. Next figure shows its circuit (see Fig. 16).

Potentiometer P1 in the feedback loop provides a variable gain which is equal to:

$$V_{ac\_amp} = -\frac{P1}{R1} V_{ac} \tag{21}$$

Values of components are selected to obtain the maximum gain of -20. The signal can be attenuated as well if the amplitude of the input signal is too high. Overall AC transfer characteristic for the maximum gain is represented next (see Fig. 17).

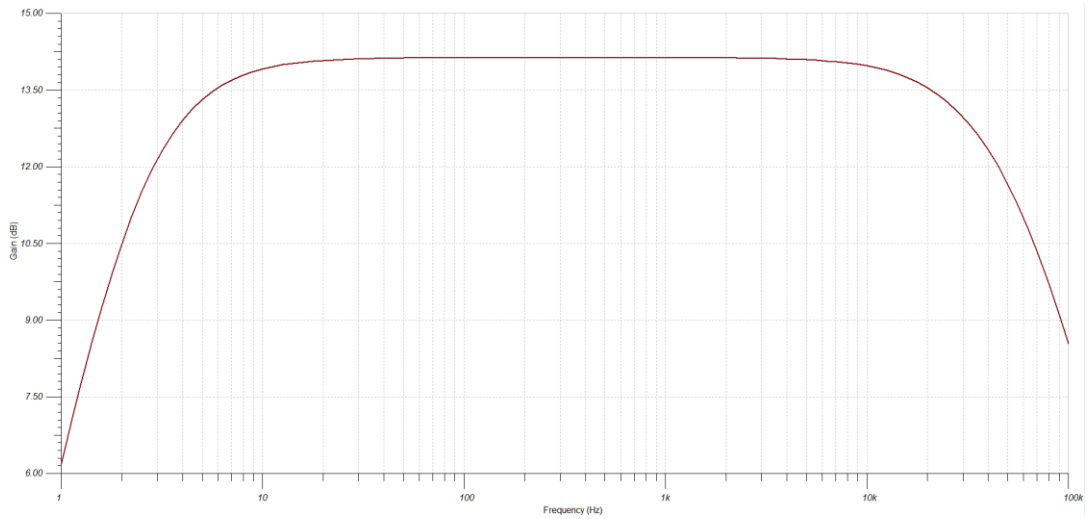

Fig. 15. AC transfer characteristic of the buffer stage.

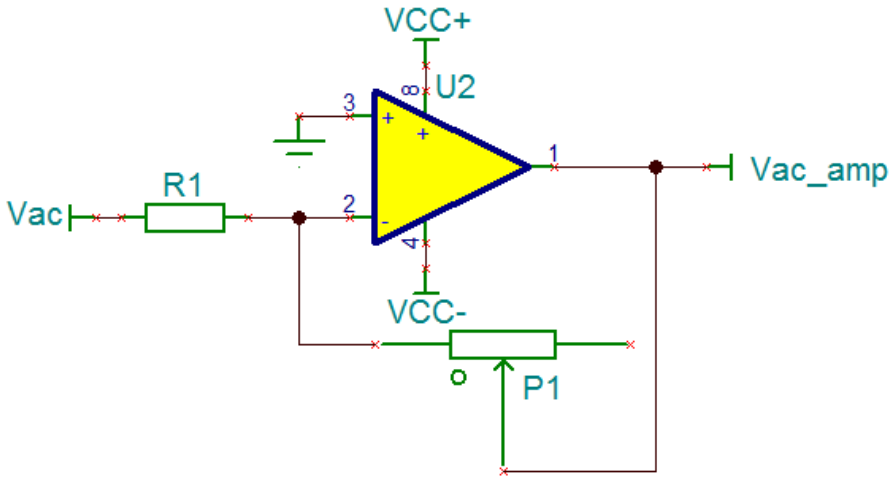

Fig. 16. Amplification stage of the conditioning circuit.

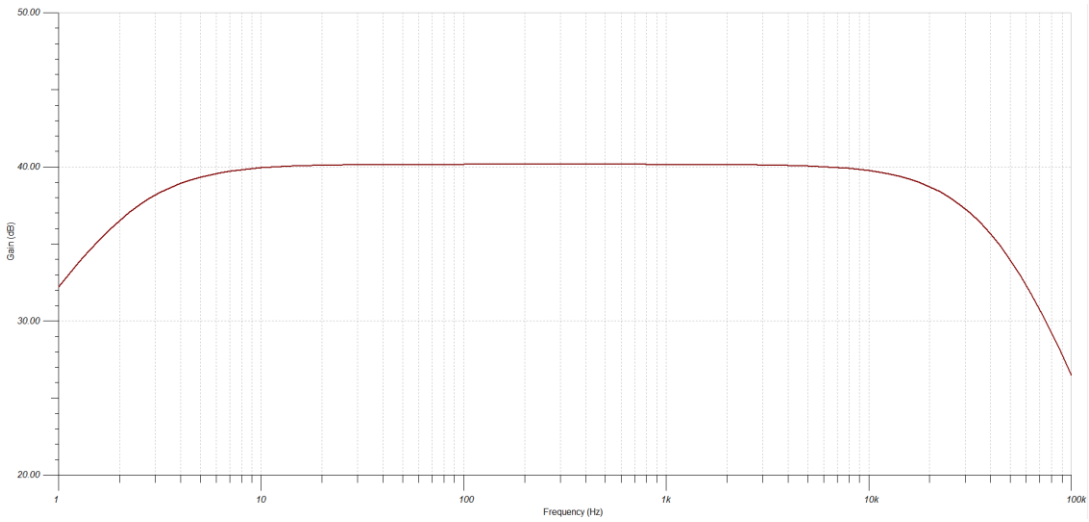

Fig. 17. AC transfer characteristic of the amplification stage.

The maximum overall amplification is equal to 101.79 V/V or 40.15 dB.

The last stage also consists of inverter amplifier as shown in the next figure (see Fig. 18).

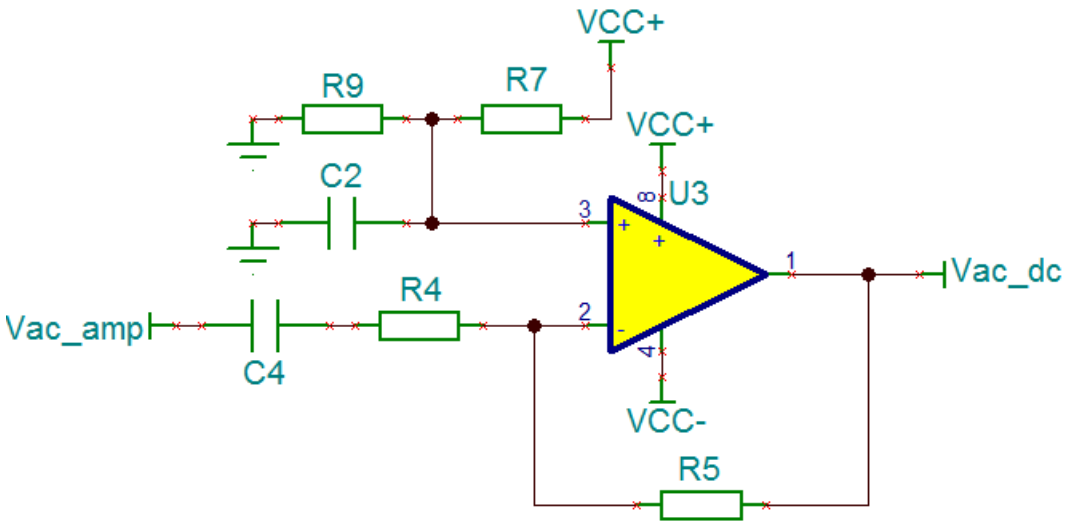

Fig. 18. DC sweep stage of the conditioning circuit.

All resistor in this stage have the same value, thus, the output signal is the inverted input signal with a DC component equal to $(VCC+)/2$. The coupling capacitor C4 rejects DC components of the input signal, whereas C2 is a decoupling capacitor and rejects AC components of the voltage divider.

Figure 19 shows the result of transient analysis at each stage.

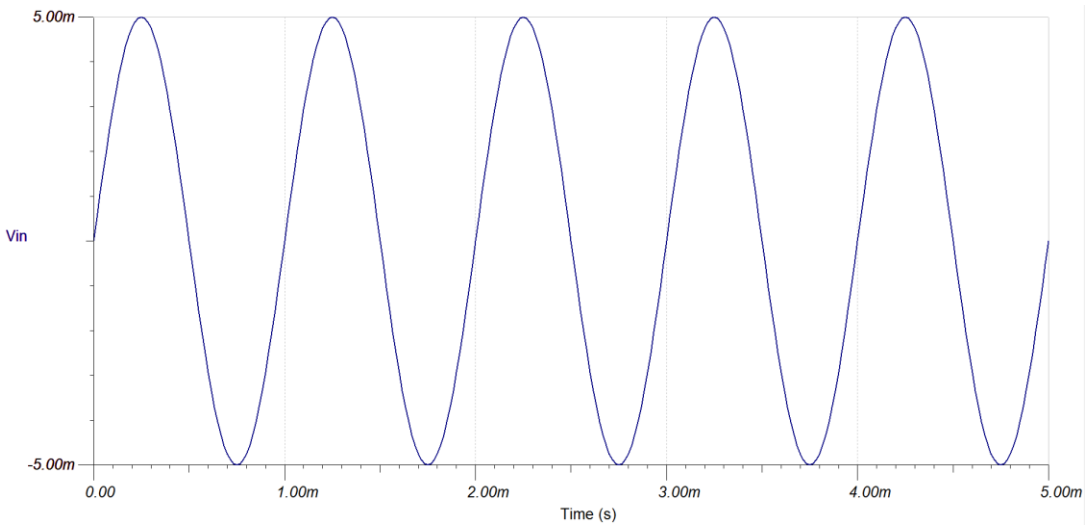

a) Input signal.

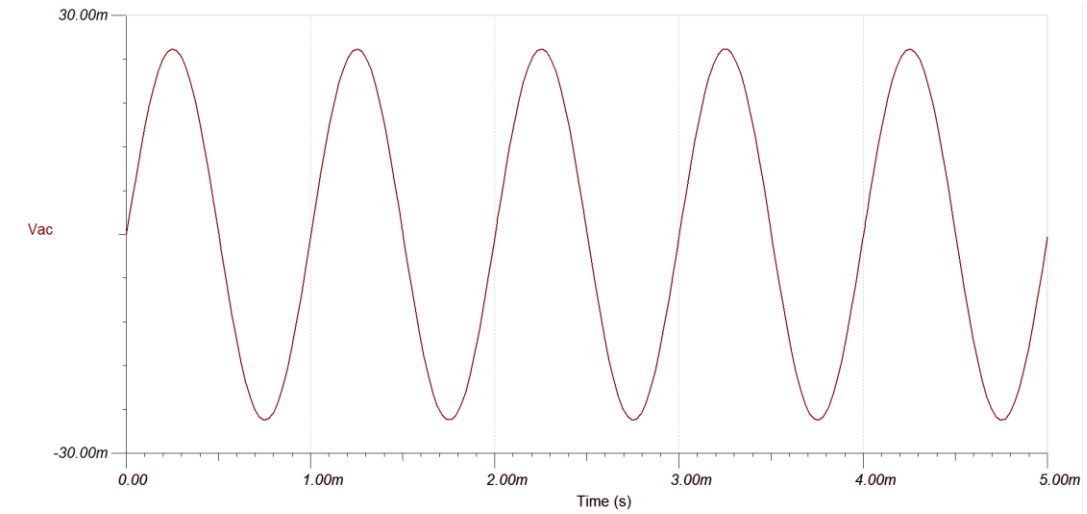

b) Output of the buffer stage.

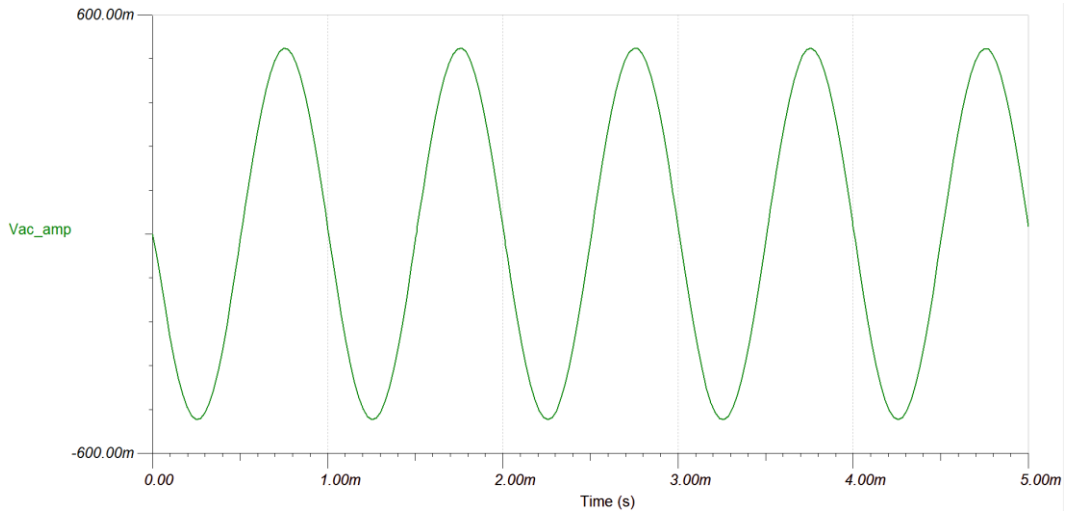

c) Output of the amplification stage.

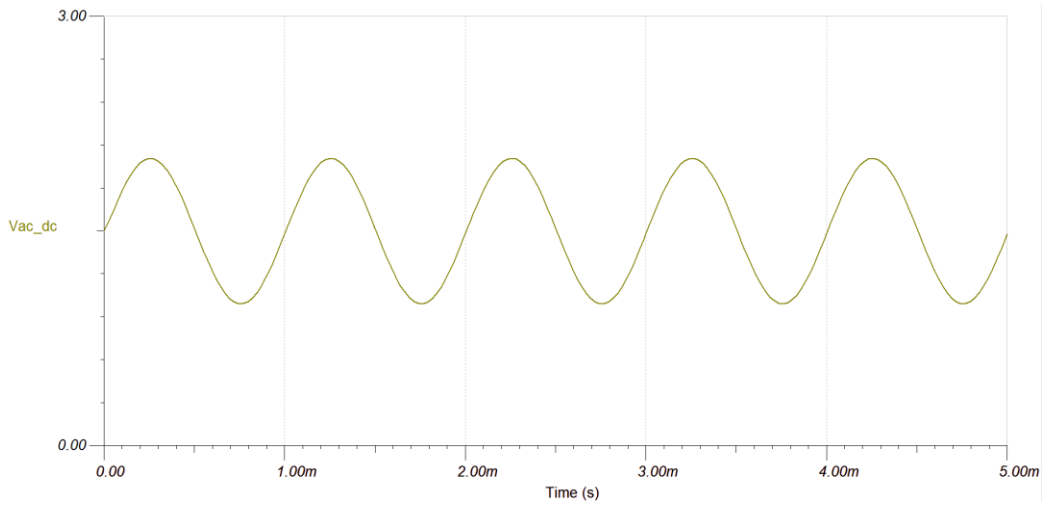

d) Output of DC sweep stage.

Fig. 19. Transient analysis.

After testing different op-amp, the OPA 703 from TI [70] was selected for U1, U2, and U3. Its principal parameters are summarized in table 5.

Tab. 5. Characteristics of the selected op-amp.

Price for 1000 pieces	€ 1.89
Operating temperature range	-40 ˚C to +85 ˚C
Rail-to-rail	Input and output
Voltage supply range	Single Supply: 4V to 12V Dual Supplies: ± 2 to ± 6
Quiescent current	160 µA
Full-scale CMRR	90 dB
Offset	160 µV
Gain-Bandwidth Product	1 MHz
Slew Rate	0.6 V/µH
Input bias current	1 pA
Available packages	SOT23-5, MSOP-8, TSSOP-14

A PCB layout of the prototype is shown in figure 20. All op-amps need a symmetrical voltage supply. Due to this, the TPS6040x for TI [71] was used. It is a 60-mA unregulated

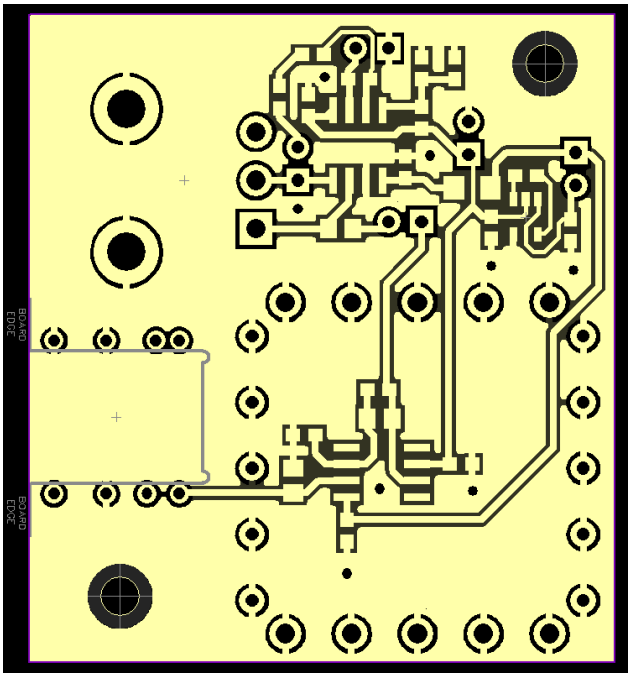

Fig. 20. Layout of the prototype PCB for the condition monitoring block.

charge pump voltage inverter. Using only three external capacitors, it generates a negative voltage from the positive input voltage. The sensor connects to the PCB by 3.5 mm jack connector. The buffering stage is shielded with a ground plane from the bottom side of PCB and a shield can from the top because of the high-value resistor connected in parallel with the sensor. It may act as an antenna and can cause EMI problems. The jack socket of the PCB and jack plug of the sensor are shielded as well. There is a jumper on the output of each stage to be able to evaluate the signal at different points of the circuit.

The prototype board and the sensor are shown in figure 21. The sensor was placed inside the enclosure for protection. The double-side non-foam tape attaches the sensor to the enclosure. To test the sensibility of the module the sensor was placed close to the heart. The captured signal in the time domain is shown in figure 22. The frequency of the signal is approximately 1.25 Hz or 75 beats a minute. The circuit is not intended to work in this frequency range, however, with an overall gain of 50V/V the signal is easily distinguishable. Next, the sensor was mounted on the AC three-phase motor which is shown in figure 23. The captured signal in the time domain is depicted in figure 24 and in the frequency domain in figure 25. The overall gain is the same. The fundamental component of the signal in the frequency domain is located at the 25.14 Hz. The rotating speed of the motor is related to the

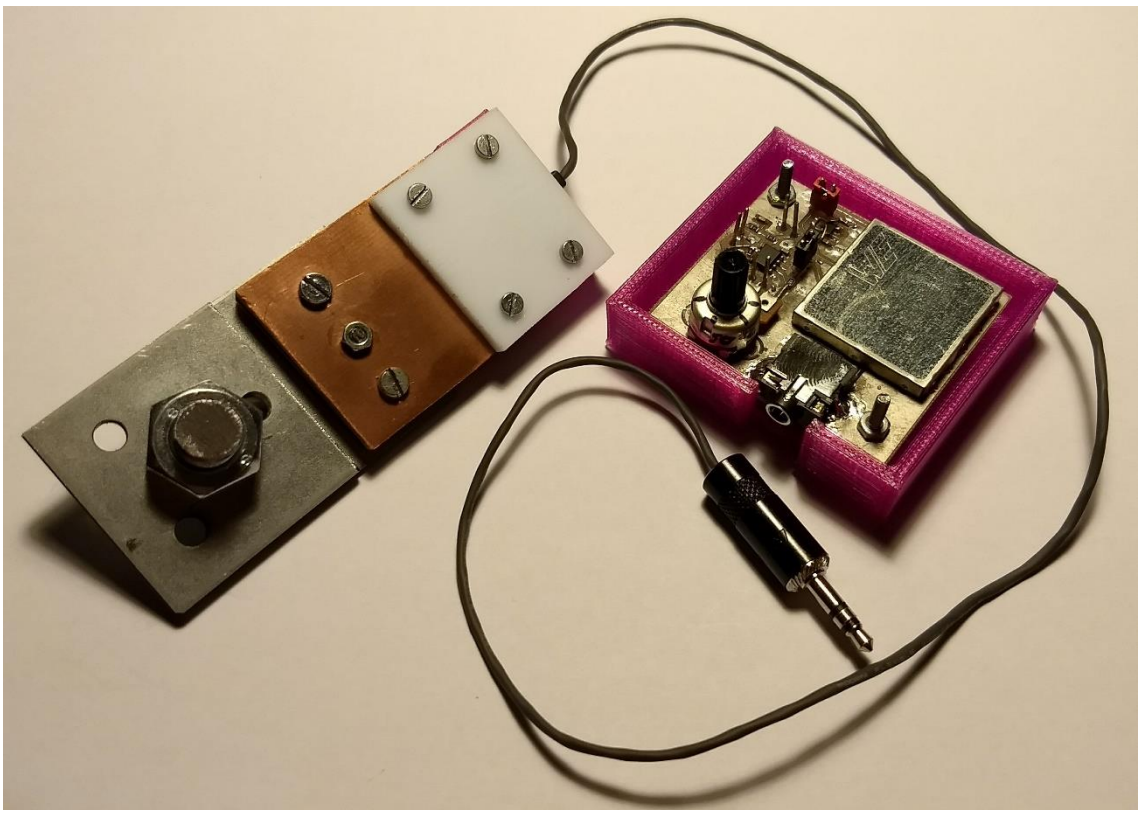

Fig. 21. Prototype board with the sensor (on the left).

frequency of fundamental component, and this case is equal to $25.14 \times 60 \approx 1508.4$ RPM. The rotating speed was confirmed with a tachometer.

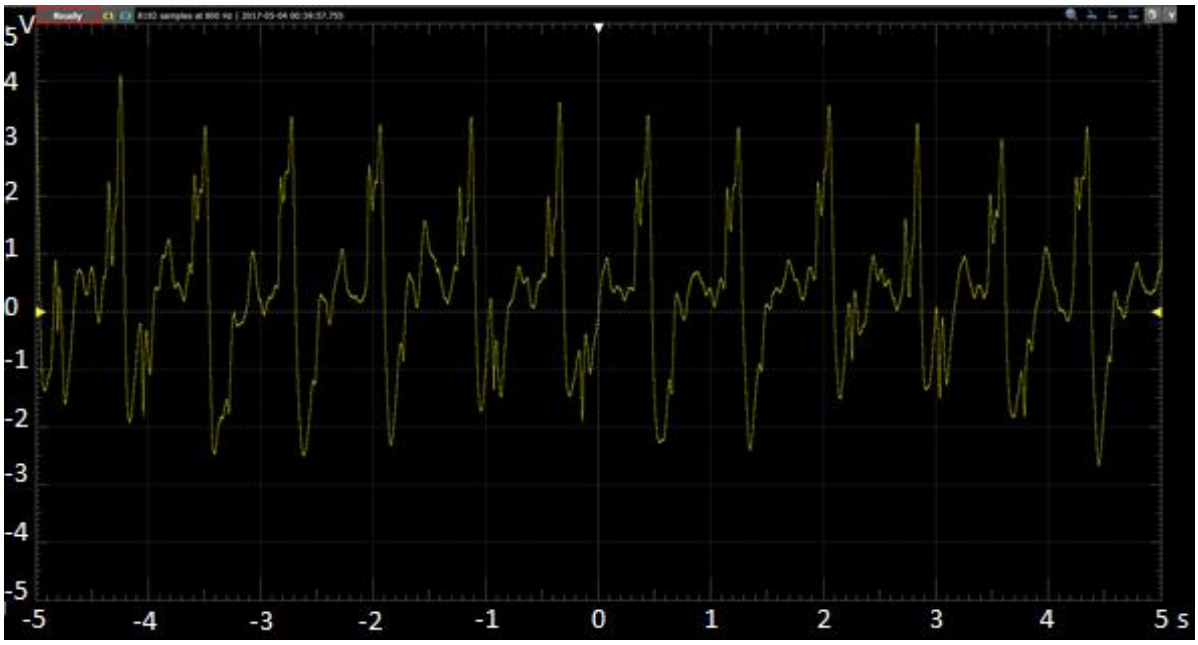

Fig. 22. Sensitivity test: heart rate sensing.

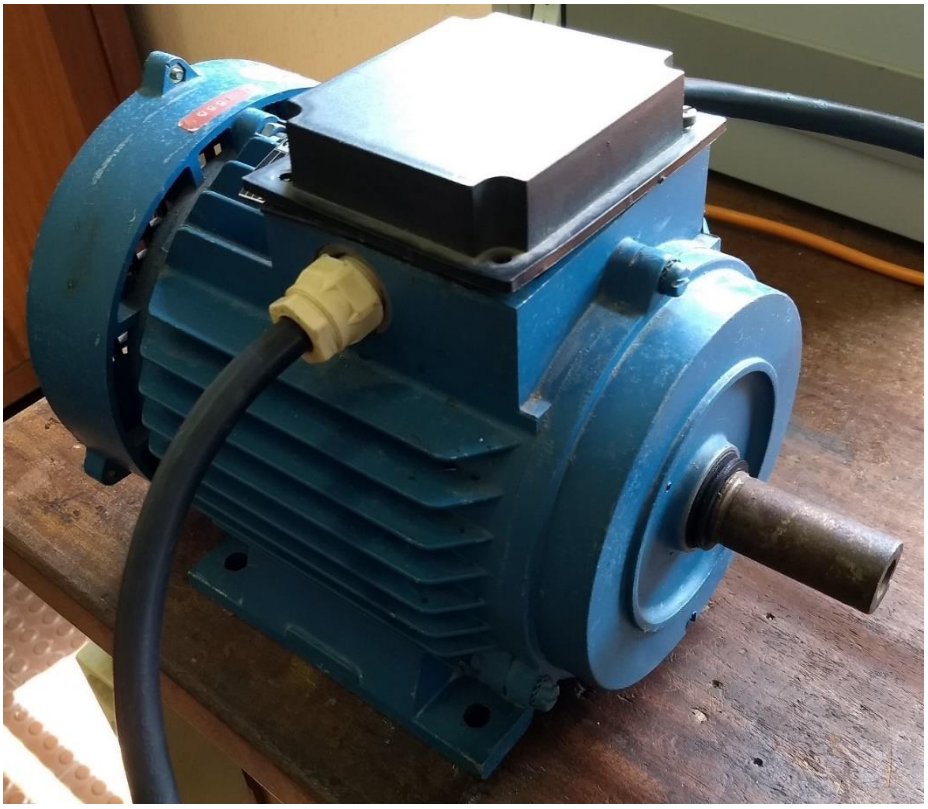

Fig. 23. Three-phase AC motor.

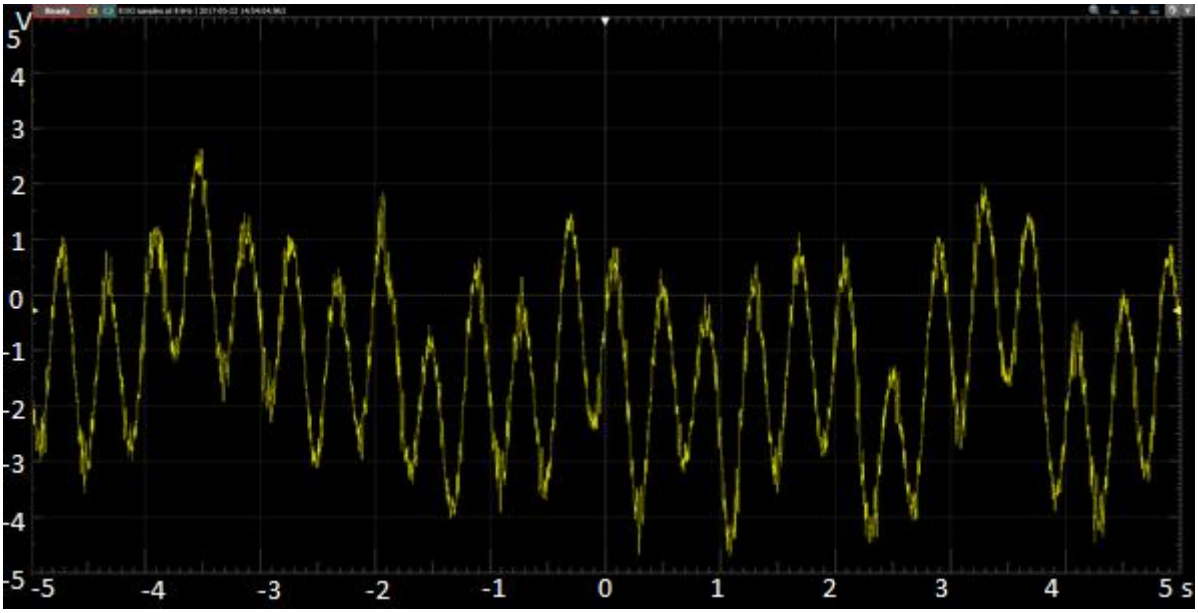

Fig. 24. Sensitivity test: AC motor's vibration sensing (time domain).

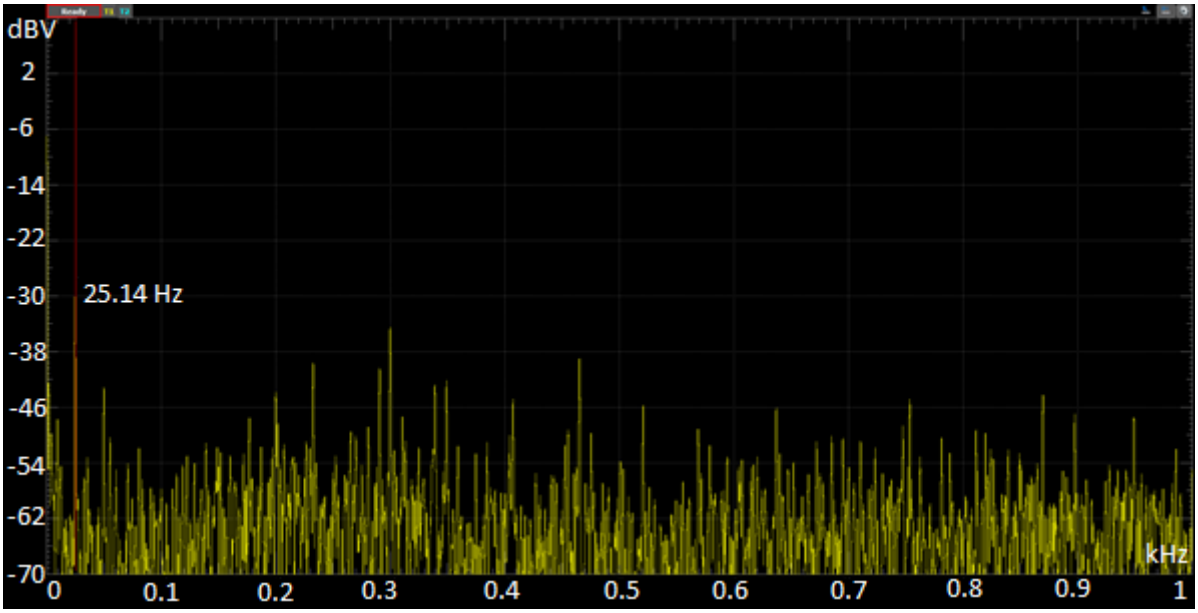

Fig. 25. Sensitivity test: AC motor's vibration sensing (frequency domain).

5. FAULT DETECTION TROUGH VIBRATION ANALYSIS

As explained in section 3.1, the vibration data obtained with the piezoelectric sensor is used for fault detection/prediction analysis. It was assumed that only the software app in the user's smartphone should trigger the vibration data recording. This is because we consider that the boat is running (and the motor is on) when the user's smartphone is on the boat and is paired with the system (via the Bluetooth connection). Therefore, it's the app that sends to the system a request for new vibration data, and not the way around. As the development of the app is out of the scope of this thesis, all the Bluetooth interface was developed and tested, but there is no actual final vibration results obtained with the complete system, as there is no Complete system available implementation for the prototype, yet, and a different strategy was used to capture the vibration data and analyze the results on vibration analysis. It was used a digital oscilloscope, a Digilent Analog Discovery 2, which is a multifunctional instrument which includes an oscilloscope, an arbitrary function generator and a digital logic analyzer. The sampling frequency, as explained earlier, is about f_s = 50 kHz, which is more than enough for the maximum signal data.

With this in mind, this chapter presents the preliminary results and discussions on the fault-detection trough vibration analysis.

5.1 TEST SET-UP FOR FAULT-DETECTION ANALYSIS

The developed electronic device and PVDF film sensor were used to capture the vibration signal. The sensor attaches to a lifting bracket of the cylinder block, which minimizes damping losses, due to the lack of gasket between the bracket and the cylinder block. The sensor is connected to the Digilent Analog Discovery 2 [72], using the conditioning circuit described in the previous chapter. Digilent Analog Discovery 2 is a multifunctional instrument, which includes an oscilloscope, arbitrary function generator, digital logic analyzer and programmable power supplies. Captured data is transferred to the computer using an USB

interface. Programmable power supplies provide symmetrical voltage for powering the conditioning circuit, and one of oscilloscope channels is used to capture the data. Each of the channels has a 14-bit resolution, 100 Ms/s maximum sampling rate, and 30 MHz bandwidth. This oscilloscope was selected to be used in this test because it supports a high bandwidth and, thus, allows to evaluate the performance of the sensor and corresponding signal conditioning circuit.

The gain of the sensor's amplifier was adjusted at the beginning of the experiment, considering that the engine is in normal condition. The data is recorded with a sampling frequency of 50 kHz. This sampling frequency was chosen to minimize aliasing. Matlab software was used for digital processing of the captured data.

The purpose of the first test was to understand how the signal changes with the rotational speed of the crankshaft. A 1.8 L four-cylinder diesel inline-four engine was used during this test. Fig. 26 demonstrates the sensor mounting.

Fig. 26. Sensor mounting.

Vibration data was captured for four different rotational speeds: 800, 1500, 2000 and 3500 revolutions per minute (RPM). A Fourier transform was used to obtain the spectrum of the signal. However, before applying the transform, a preprocessing of the signal was performed. In the first preprocessing step, the continuous component was removed, using the zero component of the Fourier transform. The next step consisted of a decimation process, which reduced the sampling rate of the signal and, consequently, its bandwidth. A low-pass filter was included in the decimation routine, to prevent aliasing resulting from the down-sampling process. This process allows us to focus on the frequencies of interest (< 12.5kHz), removing the excessive data and, thus, reducing the computational load. In this decimation process, a factor of 2 was used, in order to reduce the sampling frequency to 25 kHz, which corresponds to a 12.5 kHz bandwidth, according to the Nyquist–Shannon theorem.

Figures 27-30 present the results of the spectrum, for each rotational speed. Regardless of the rotational speed of crankshaft, it is important to note that the developed module can always provide sufficient bandwidth for signal capture, as the maximum sampling frequency allowed in the microprocessor and A/D converter is 1M sample/s (much higher than the 25kHz needed).

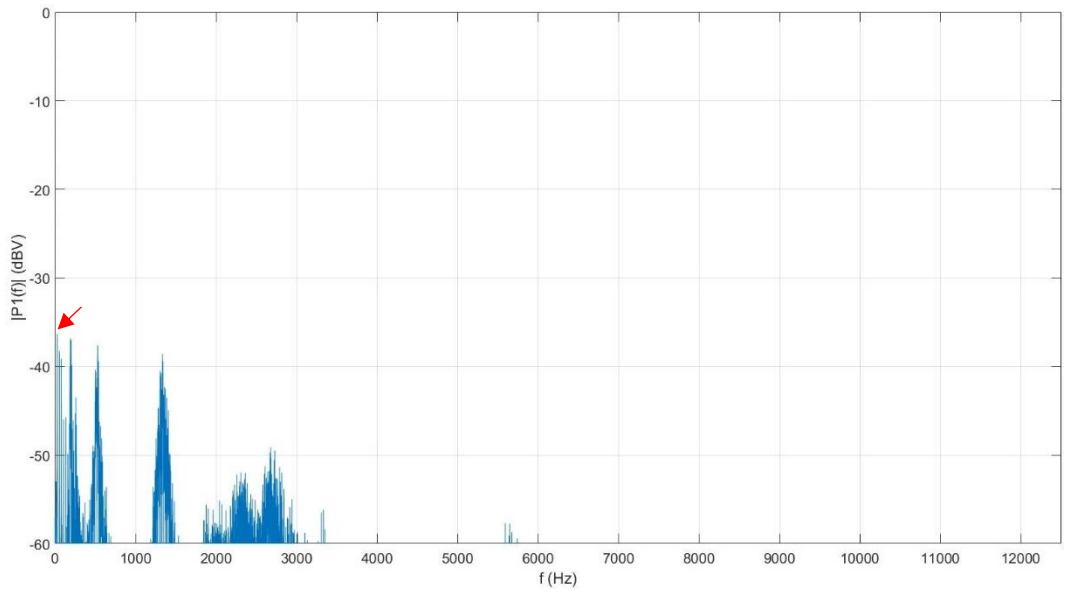

Fig. 27. Spectrum of the signal for 800 RPM.

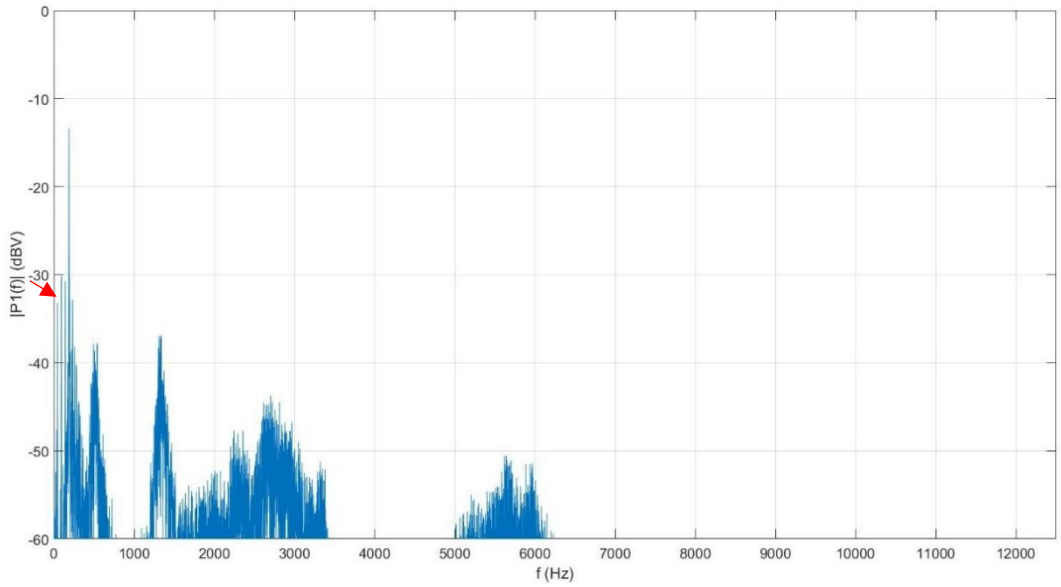

Fig. 28. Spectrum of the signal for 1500 RPM.

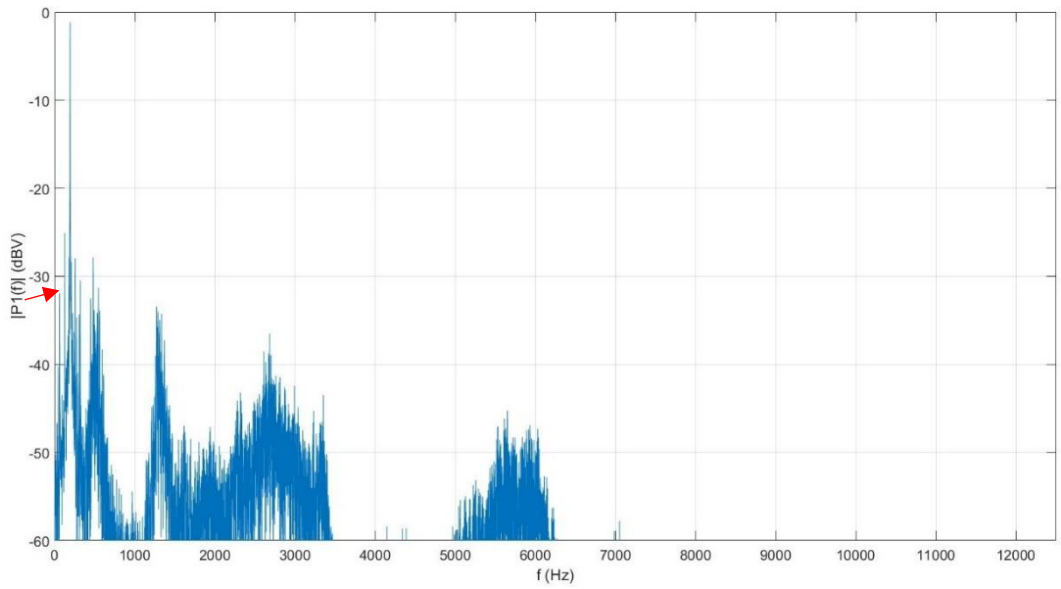

Fig. 29. Spectrum of the signal for 2000 RPM.

It can be seen from Fig. 27-30 that the engine's vibration signal is a multi-frequency signal with a very large number of frequencies present. There are fixed and variable frequency components. The amplitude of the fixed components increases with rotational speed, as well as the noise level. The main fixed components are situated in 193, 530 and 1330 Hz. Variable frequency components are related with moving mechanisms. The engine is one of such mechanisms, and the prime source of these frequency components, because it generates a complete set of harmonics. The fundamental component, or the first harmonic (indicated by the red arrow in figures) is equal to twice the crankshaft rotational speed. Other harmonics are

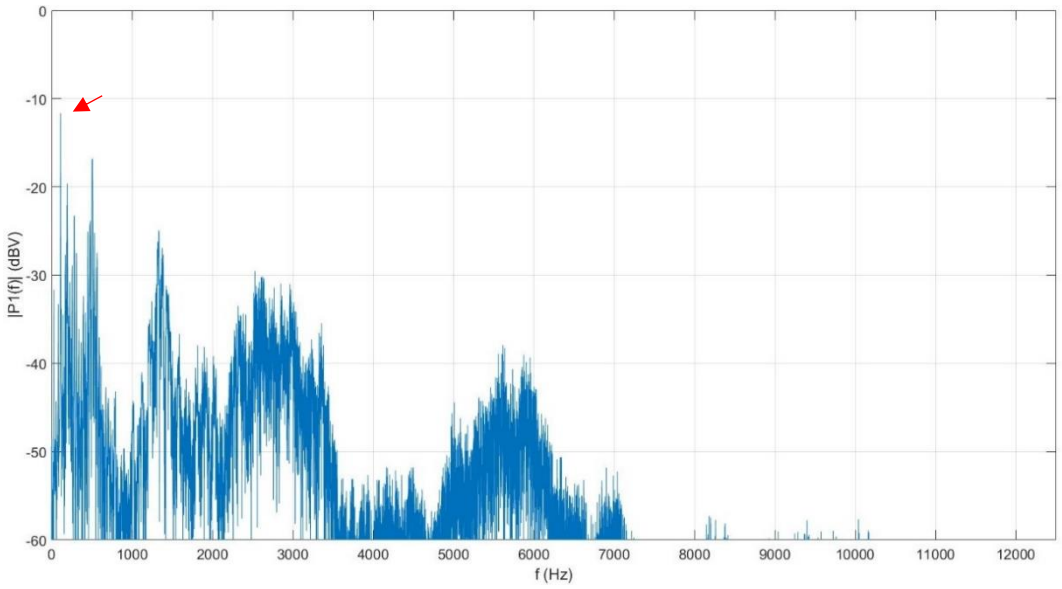

Fig. 30. Spectrum of the signal for 3500 RPM.

multiples of this fundamental component. The first harmonic is not always the dominant component of the spectrum (see fig. 29), and its identification, sometimes, is not a trivial task. The portion of the spectrum shown in figure 31 illustrates this problem. According with this data, each of the first four signal peaks (in 28, 56, 85 or 113 Hz) can be a fundamental harmonic.

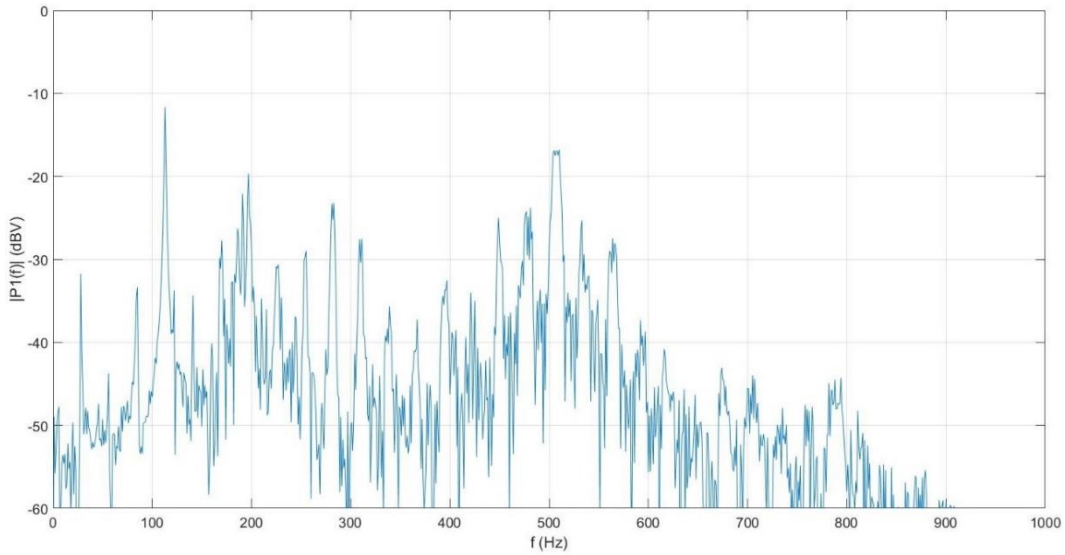

Fig. 31. Enlarged portion of the spectrogram.

Moreover, the presence of non-integer harmonics is common in 4-stroke engines (e.g. 0.25, 0.5, 1.5, 2.5…) and the associated component cannot be identified by peaks' multiplicity, or

by its least common multiple. Each of the mentioned peaks has three “harmonics”, which are, actually, non-integer harmonics of the true fundamental component (113 Hz). In resume, this can show us how complex is the engine vibration signal and, consequently, its analysis.

5.2 DATA ANALYSIS AND METHODS FOR FAULT DETECTION

To obtain vibration data associated with each type of fault, two distinct types of faults were forced in a 1.4 L four-strokes petrol inline-four engine. The simulated faults comprised a blocked injector and the absence of spark in a cylinder. The blocked fuel injector was simulated by switching off the command signal of the corresponding injector, which stops the delivery of the fuel mixture to that cylinder. The lack of spark in the cylinder is simulated by switching off the high-voltage cable between the spark plug and the ignition coil or magneto. The result of each fault is the same – the absence of combustion in the cylinder. The sensor was attached to a lifting bracket of the cylinder block next to the fourth cylinder. Each of the faults was simulated in two cylinders: one closest to the sensor and the other distant from it.

A Fourier transform was used to obtain the spectral representation of the signal. Figure 32 shows the frequency spectrum of the signal for a normal operating state of the engine. According to the spectrum, the useful maximum frequency of the signal is 5 kHz.

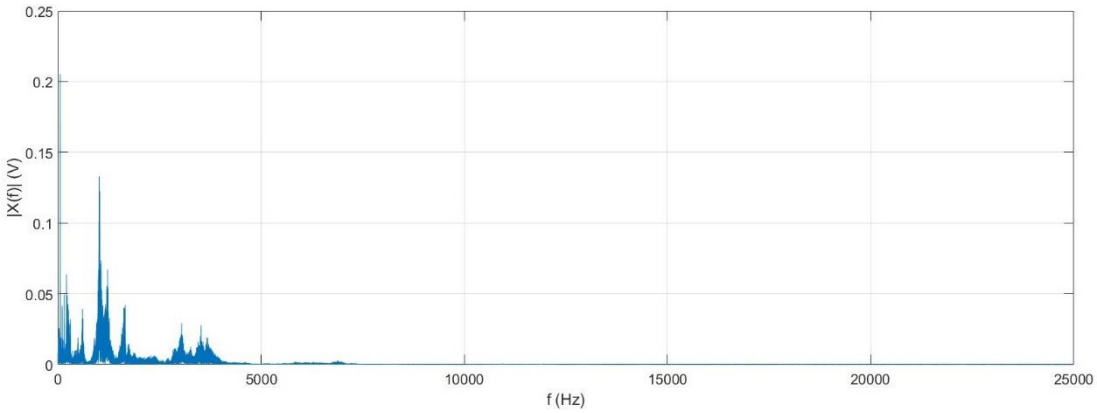

Fig. 32. The spectrum of the captured vibration signal.

5.2.1 TIME DOMAIN

Figures 33-35 show the preprocessed signal in the time domain, respectively considering a normal condition and two simulated faults (distant cylinder).

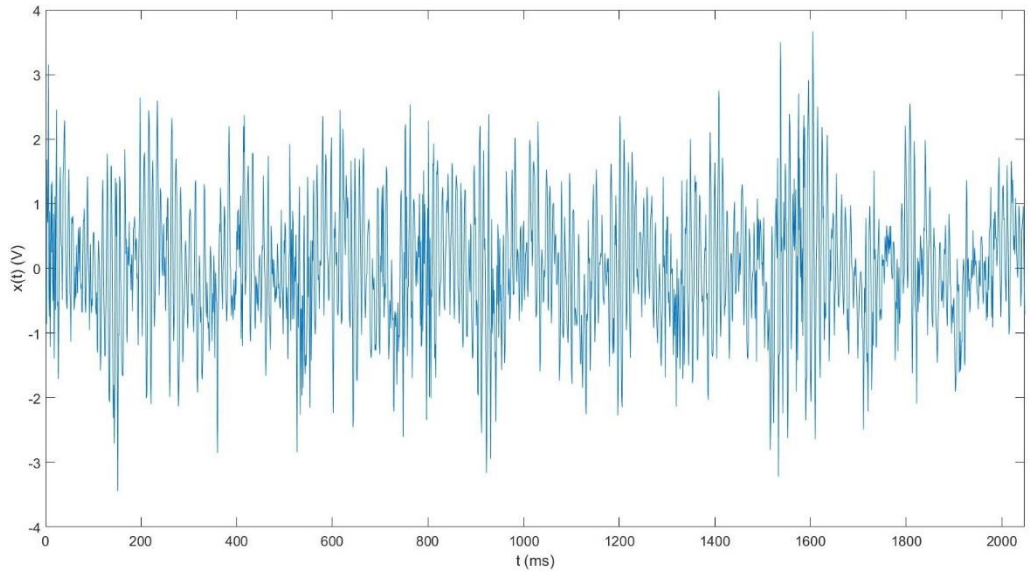

Fig. 33. Normal condition, time domain.

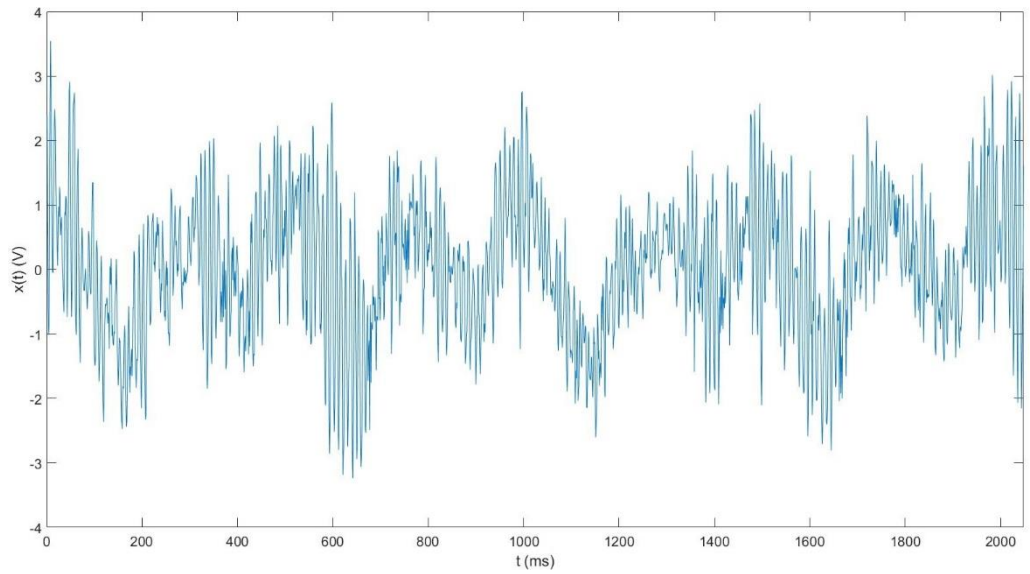

Fig. 34. Lack of spark in the first cylinder, time domain.

In a fault condition, the dominant component becomes clearer. However, the overall amplitude in all cases is nearly the same due to the presence of noise and other signal components. This type of analysis allows the tracking of the signal variation, but all

components of the signal are always present. Because of it, the fault detection in the time domain is difficult. Components can be separated by filtering, and this concept is somewhat similar to the idea of the discrete wavelet transform.

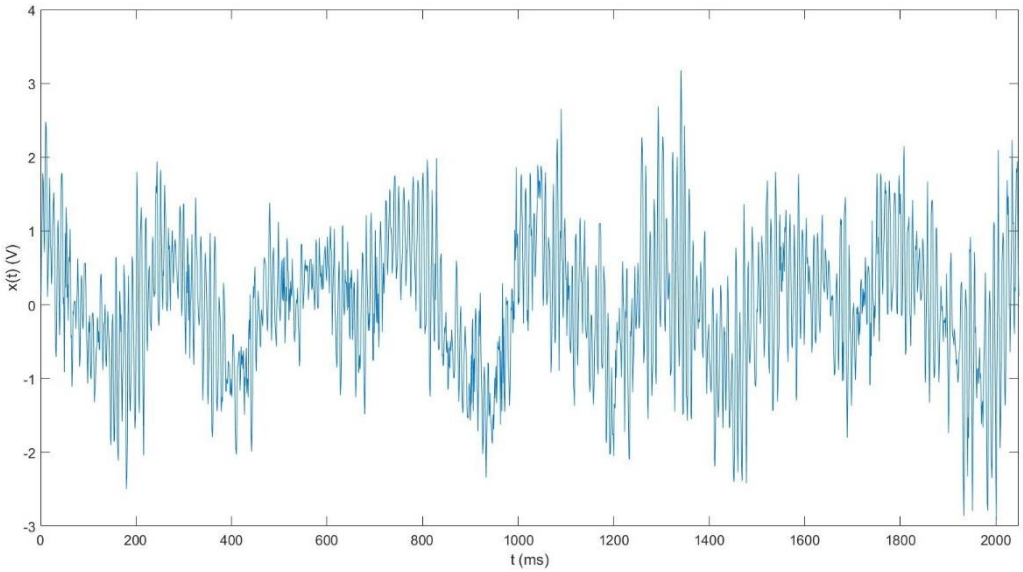

Fig. 35. Blocked injector in the first cylinder, time domain.

5.2.2 FREQUENCY DOMAIN

In this stage, the preprocessed signal of each condition was converted from the time domain to the frequency domain by applying a Fourier transform. Results of the transform are depicted in figures 36-38. As can be verified, the spectrum maintains its shape in all conditions. Both frequency and amplitude of the fundamental component (indicated by red arrow) change when a fault occurs. However, the frequency of the first harmonic in both faults is the same, which can be explained by the fact that simulated faults are similar in terms of consequences. Another notable difference is a reduction in the amplitude of harmonics between 150 and 320 Hz. Although, variation in the rotational speed of the crankshaft can cause some of these changes.

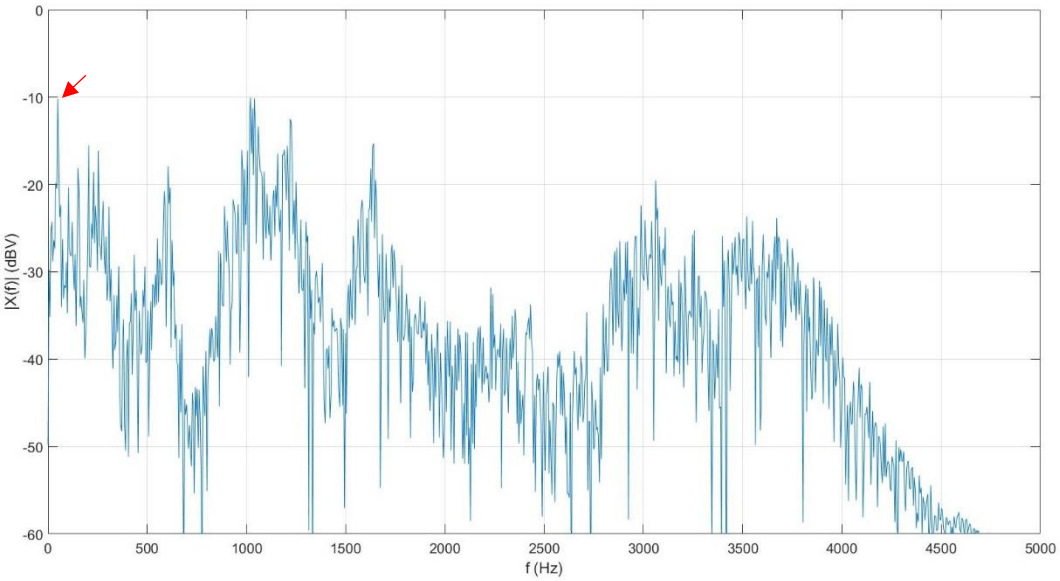

Fig. 36. Normal condition, frequency domain.

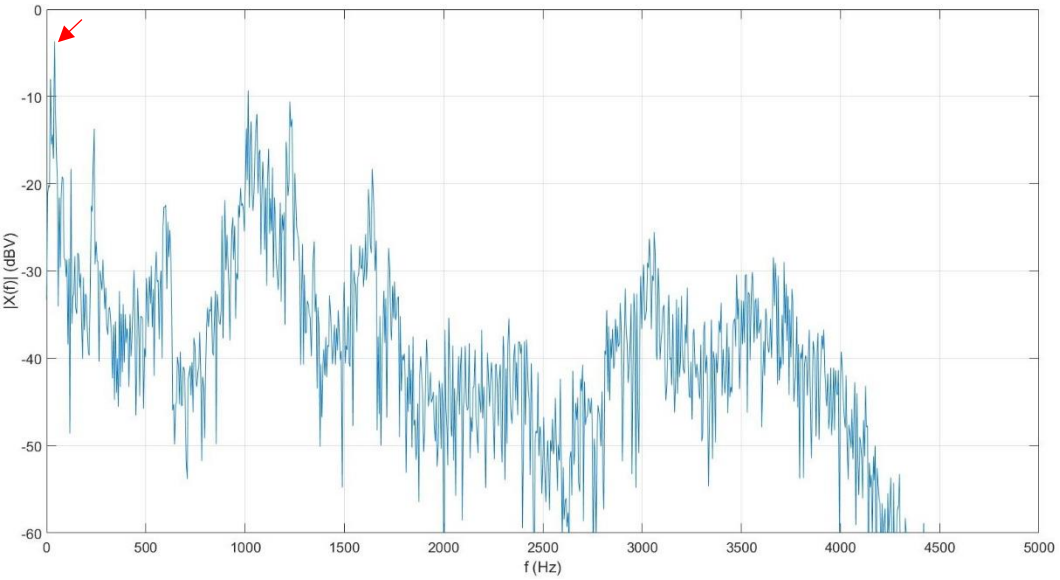

Fig. 37. Lack of spark in the first cylinder, time domain.

The analysis in the frequency domain allowed the identification of more differences between the normal condition and the faulty one. However, the difference between these two conditions is not evident. In contrast with the analysis in the time domain, it is possible to compare individual components of the signal as it is decomposed into the series of basic terms (in this case sinusoids). However, the information about signal variation over the time is lost as it is contained in the phase and only the modulus is considered.

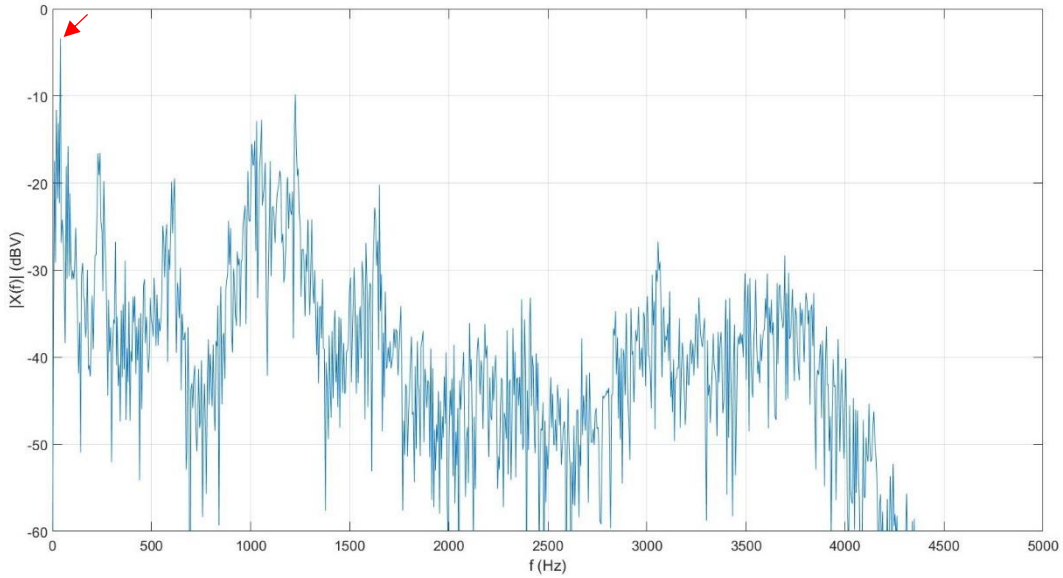

Fig. 38. Blocked injector in the first cylinder, time domain.

5.2.3 TIME-FREQUENCY METHODS' COMPARISON

TF analysis combines the advantages of time and frequency domain analyses. It allows the tracking of individual components of the signal as they occur with the time which might improve the classification of the signal.

Before applying TF methods, the signal is transformed into the analytical form by applying a Hilbert transform. The analytical form allows the reduction of cross-terms that appear in some TF methods. After preprocessing the signal, a TF method can then be applied. For this purpose, the Time-frequency toolbox of MATLAB [73] is used. The following list shows the methods used in the tests with the corresponding abbreviations:

- Short-time Fourier transform (STFT)
- Born-Jordan distribution (BJ)
- Butterworth distribution (BUD)
- Choi-Williams distribution (CW)
- Margenau-Hill spectrogram distribution (MHS)
- Pseudo Margenau-Hill distribution (PMH)
- Pseudo Wigner-Ville distribution (PWV)
- Reduced interference distribution with Bessel window (RIDB)
- Reduced interference distribution with binomial window (RIDBN)

- Reduced interference distribution with Hanning window (RIDH)
- Reduced interference distribution with triangular window (RIDT)
- Fourier spectrogram distribution (SP)
- Smoothed Pseudo Wigner-Ville distribution (SPWV)
- Wigner-Ville distribution (WV)
- Zhao-Atlas-Marks distribution (ZAM)
- Morlet Wavelet scalogram (MSC)

The evaluation of the effectiveness of these methods to perform the identification of faults was made using the visual analysis and the Rényi entropy. The former is used to estimate signal information and complexity in the time-frequency plane [47]. It reflects the number of well-separated components of the signal and provides an adequate metric for comparing results with the different methods. In this particular case, a logarithm of base two is used, yielding a result that is expressed in bits, and like in [46], a Rényi entropy of second order was used for tests.

Both digital preprocessing and processing stages were automated to get comparable results for all methods, and each engine condition.

The experimental results are summarized in table 6. Each line represents one of the tested methods and includes the Rényi information for different conditions, as well as the required computational time. Five conditions are shown: Normal – no faults, Sp1 – no spark on the first cylinder, Sp4 - no spark on the fourth cylinder, Inj1 – blocked fuel injector in the first cylinder, Inj4 – blocked fuel injector in the fourth cylinder. The Rényi information value differs according with each condition, which is caused by variation of the number of components of the signal. The greater the variation between the two conditions, the easier it is to distinguish them.

For easier evaluation of the results obtained by the different methods and for each fault, Figs. 39-42 present the charts showing the absolute difference of Rényi information between the normal condition and the corresponding faulty condition. The charts combine a bar graph, which represents the Rényi information of the compared conditions and the line graph, which represents the absolute difference between two conditions. The horizontal axis represents the name of the methods, which is common for both graphs. The left horizontal axis is for bar graph, and the right one is for the line graph.

Tab. 6. Values obtained from the TF methods for each of the induced faults.

Method	Rényi Entropy					Comp. Time
	Normal	Sp1	Sp4	Inj1	Inj4	
BJ	5.159	4.565	4.854	4.657	4.429	4.209s
BUD	5.395	4.736	5.020	4.832	4.529	4.533s
CW	5.476	4.784	5.071	4.881	4.557	4.579s
MHS	6.368	5.665	5.938	5.824	5.386	0.148s
PMH	5.157	4.721	4.890	4.766	4.651	0.086s
PWV	3.597	3.277	3.349	3.241	3.246	0.090s
RIDB	5.033	4.485	4.762	4.574	4.372	4.750s
RIDBN	4.605	4.131	4.396	4.229	4.153	6.725s
RIDH	4.900	4.388	4.658	4.477	4.309	5.061s
RIDT	4.939	4.421	4.691	4.506	4.329	4.559s
MSC	17.283	15.659	15.738	15.700	14.827	35.347s
SP	6.385	5.583	5.854	5.692	5.206	0.150s
SPWV	5.654	4.878	5.167	4.979	4.615	4.421s
STFT	8.454	7.943	8.147	7.959	7.846	0.130s
WV	0.651	0.501	0.481	0.384	0.408	0.172s
ZAM	4.024	4.883	4.484	4.880	4.928	4.112s

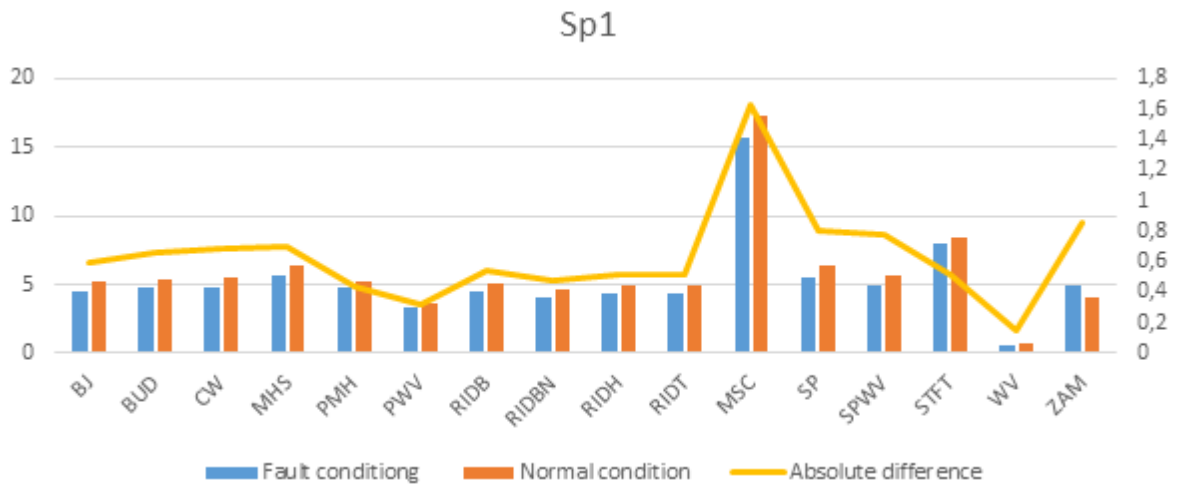

Fig. 39. Rényi entropy for normal condition and Sp1 fault calculated by each of the methods.

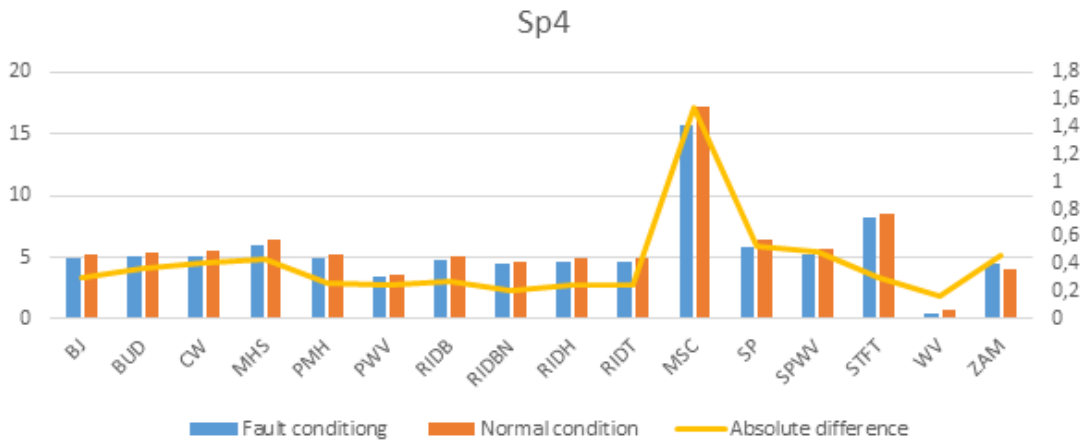

Fig. 40. Rényi entropy for normal condition and Sp4 fault calculated by each of the methods.

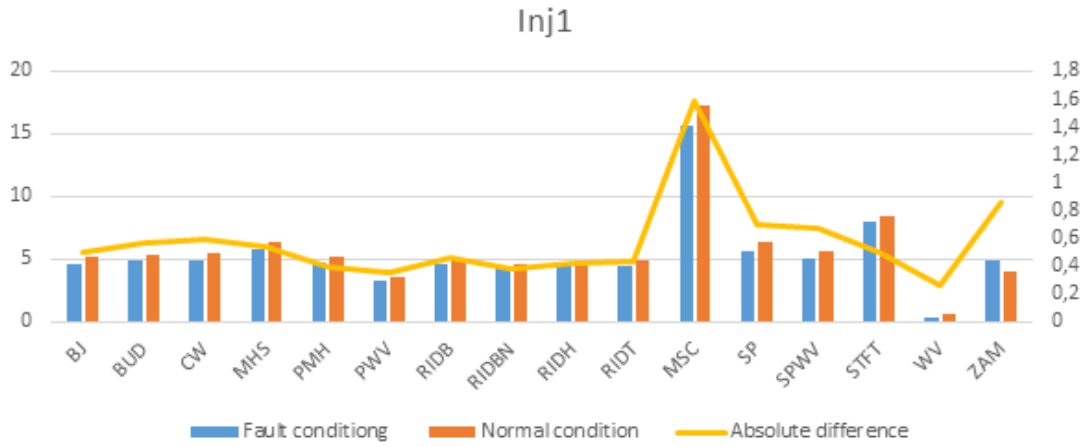

Fig. 41. Rényi entropy for normal condition and Inj1 fault calculated by each of the methods.

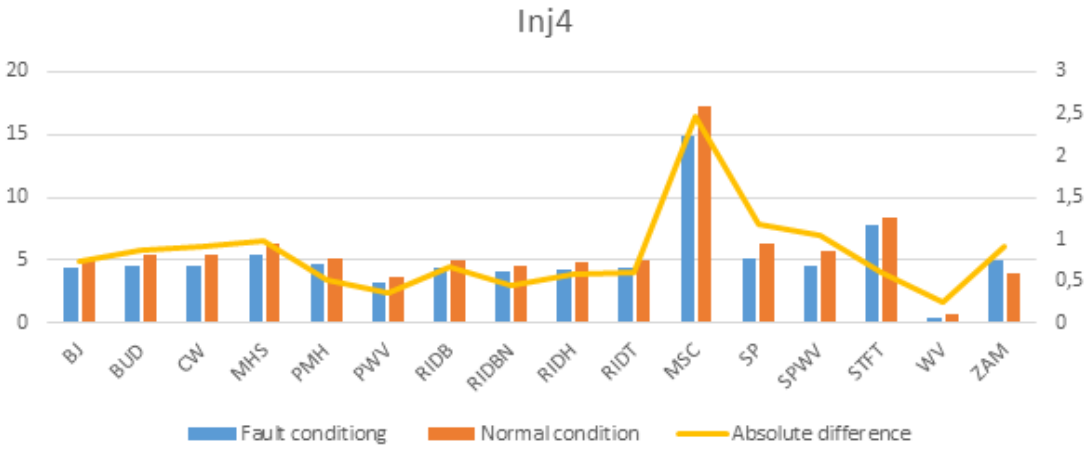

Fig. 42. Rényi entropy for normal condition and Inj4 fault calculated by each of the methods.

In all cases, the Morlet scalogram method gave the maximum difference. Its difference is considerably higher when compared with the other methods. At the same time, the WVD method gave the minimum difference, in all faults. Regarding the other methods, they show similar results. However, the results of the SP, SPWV and ZAM methods had greater variations. SP and SPWV had similar differences.

The visual analysis confirms most of these results. The better and worst methods remain the same. Figure 43 shows both the Morlet scalogram for normal and faulty conditions. Figure 44 shows the WVD method also for normal and faulty conditions. While the difference between normal and faulty condition is hard to distinguish in the case of the WVD method, in the case of Morlet scalogram the difference between these two conditions is clear. According to the visual analysis, the ZAM method demonstrated better results than SP or SPWV, for all of the conducted tests. Also, SPWV always provided better TF resolution that SP. These observations can be confirmed by inspecting figures 45-47 which allow the comparison of the TF resolution of the mentioned methods when a fault in Inj. 4 occurs. The final difference concerns the position of the MHS with respect to the other methods. Despite the interference terms, BJ, BUD, and CW provide better TF resolution when compared with the MHS. Figures 48-51 allow the comparison of the TF resolution of these methods when a fault occurs in Inj. 4.

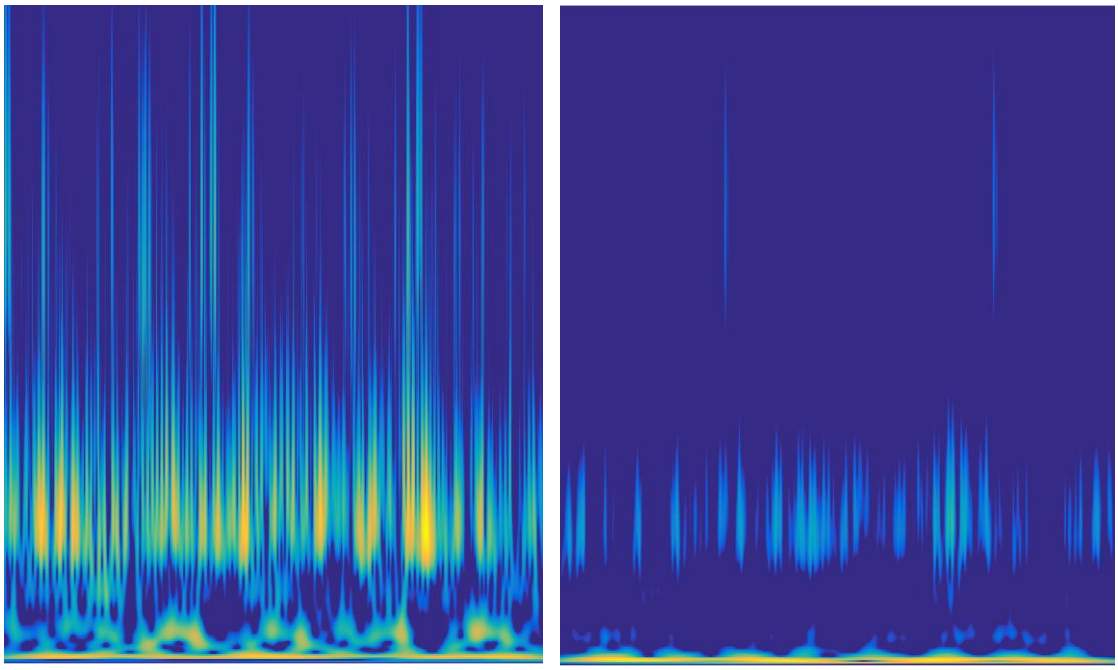

Fig. 43. Morlet scalogram: normal condition (left side), blocked fuel injector in the fourth cylinder (right side).

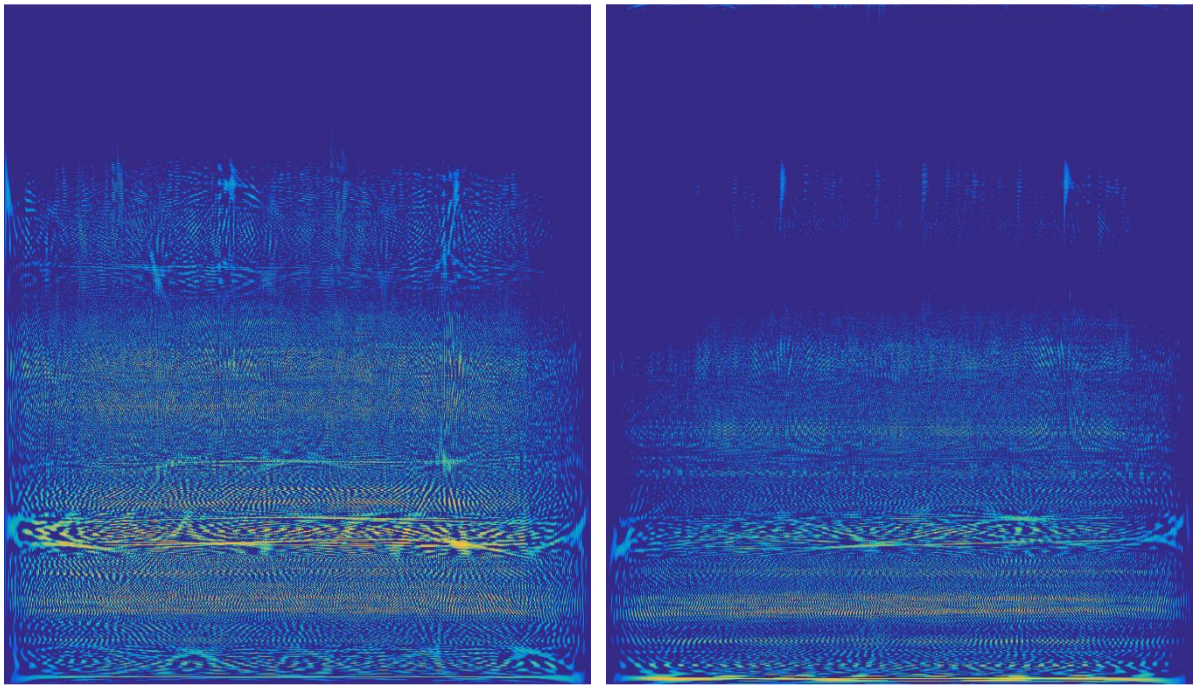

Fig. 44. WVD: normal condition (left side), blocked fuel injector in the fourth cylinder (right side).

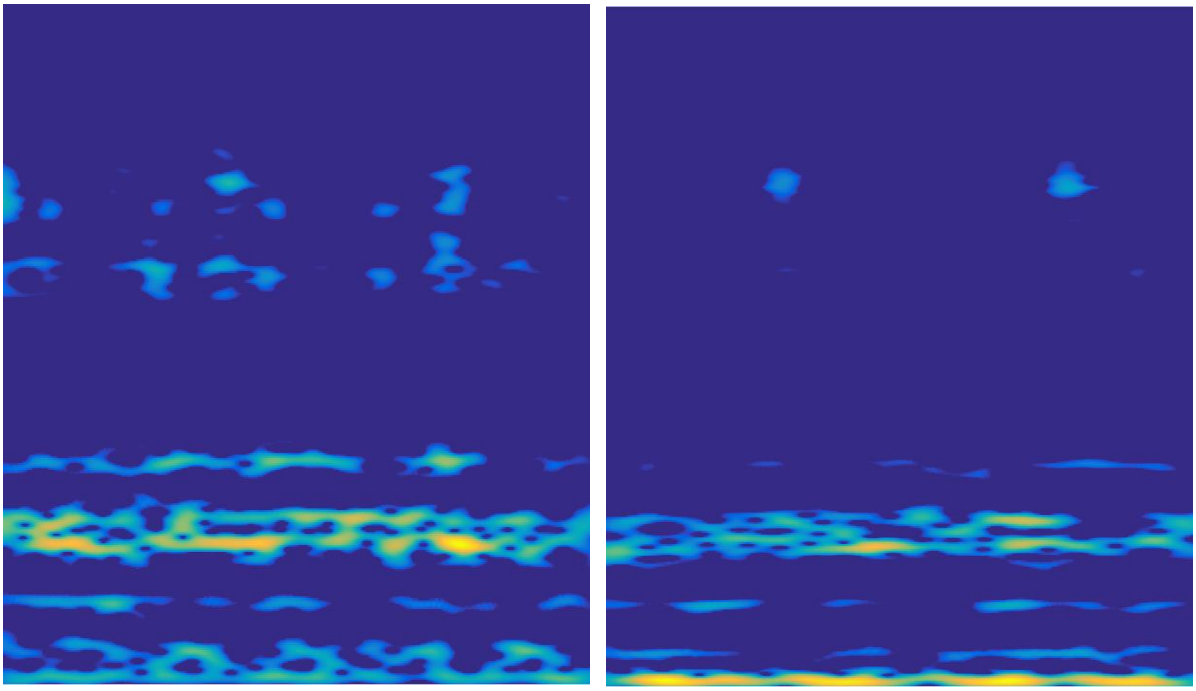

Fig. 45. SP: normal condition (left side), blocked fuel injector in the fourth cylinder (right side).

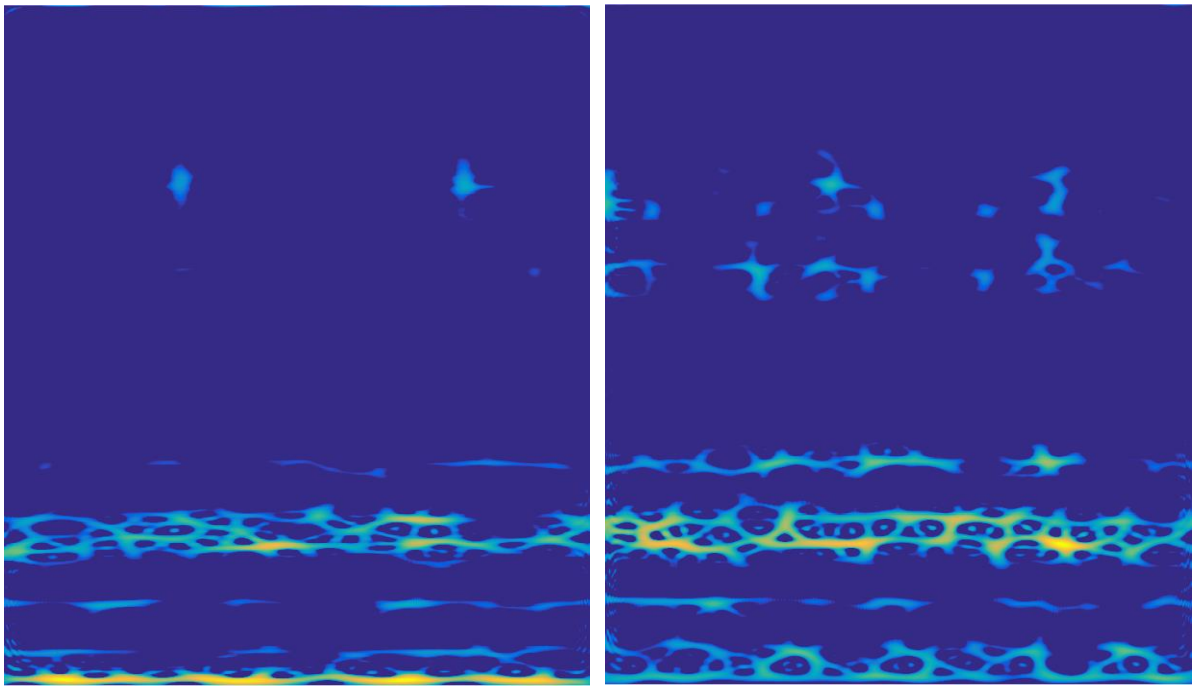

Fig. 46. SPWV: normal condition (left side), blocked fuel injector in the fourth cylinder (right side).

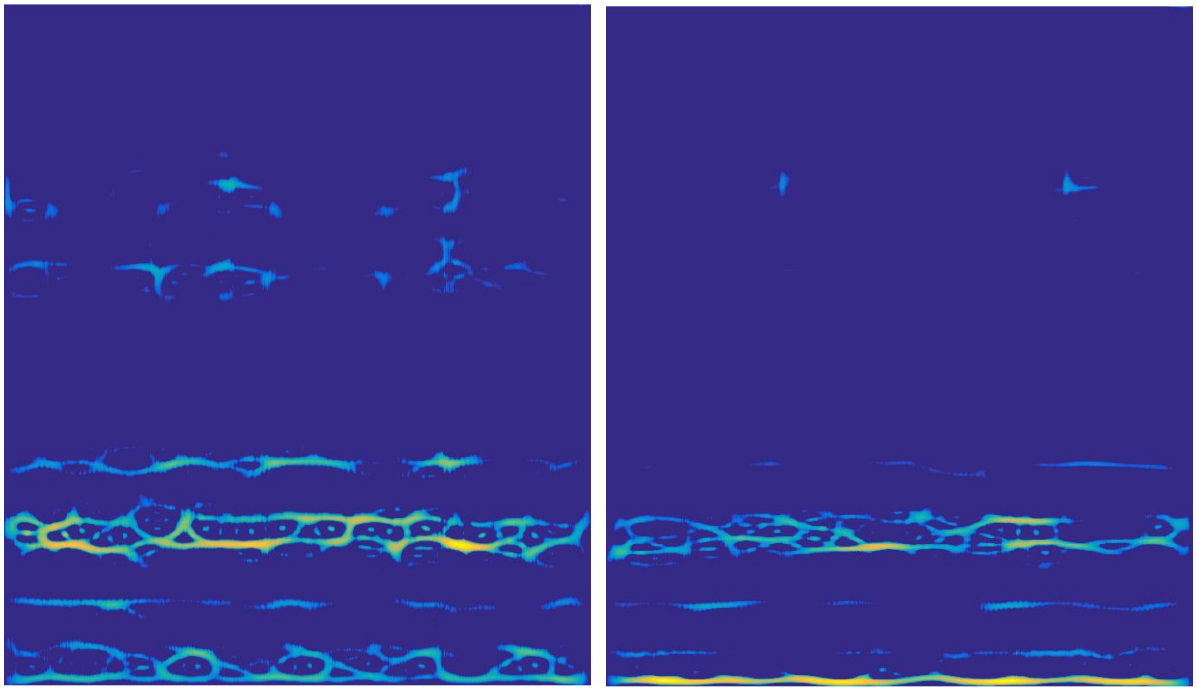

Fig. 47. ZAM: normal condition (left side), blocked fuel injector in the fourth cylinder (right side).

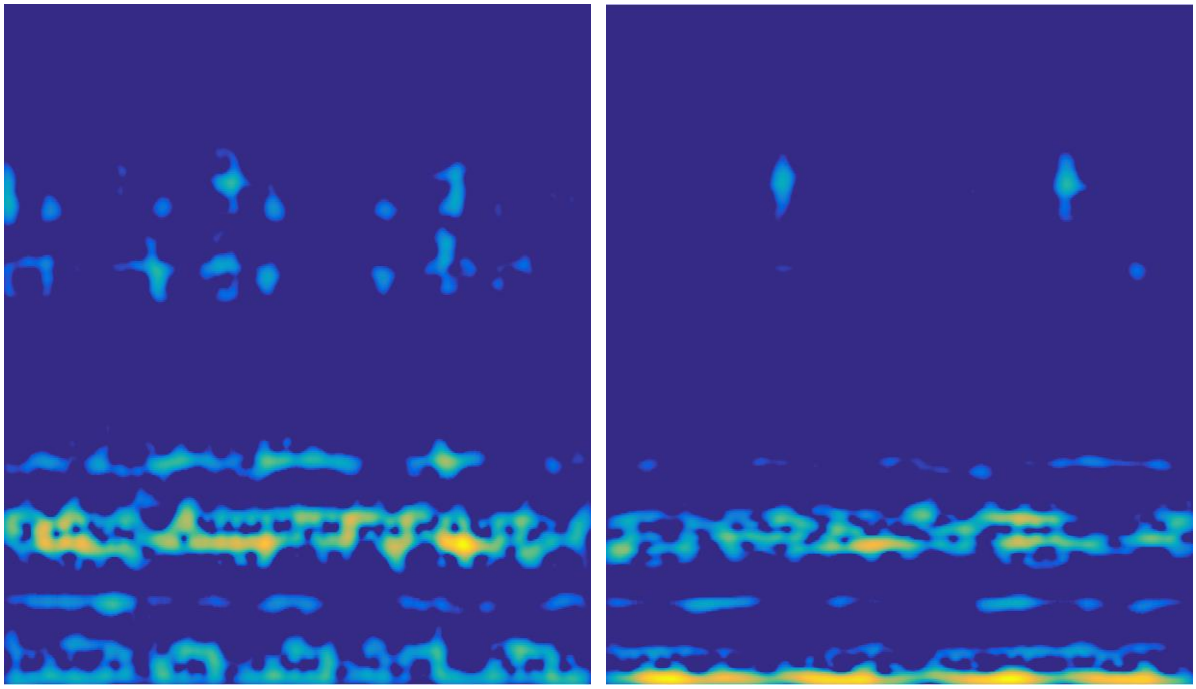

Fig. 48. MHS: normal condition (left side), blocked fuel injector in the fourth cylinder (right side).

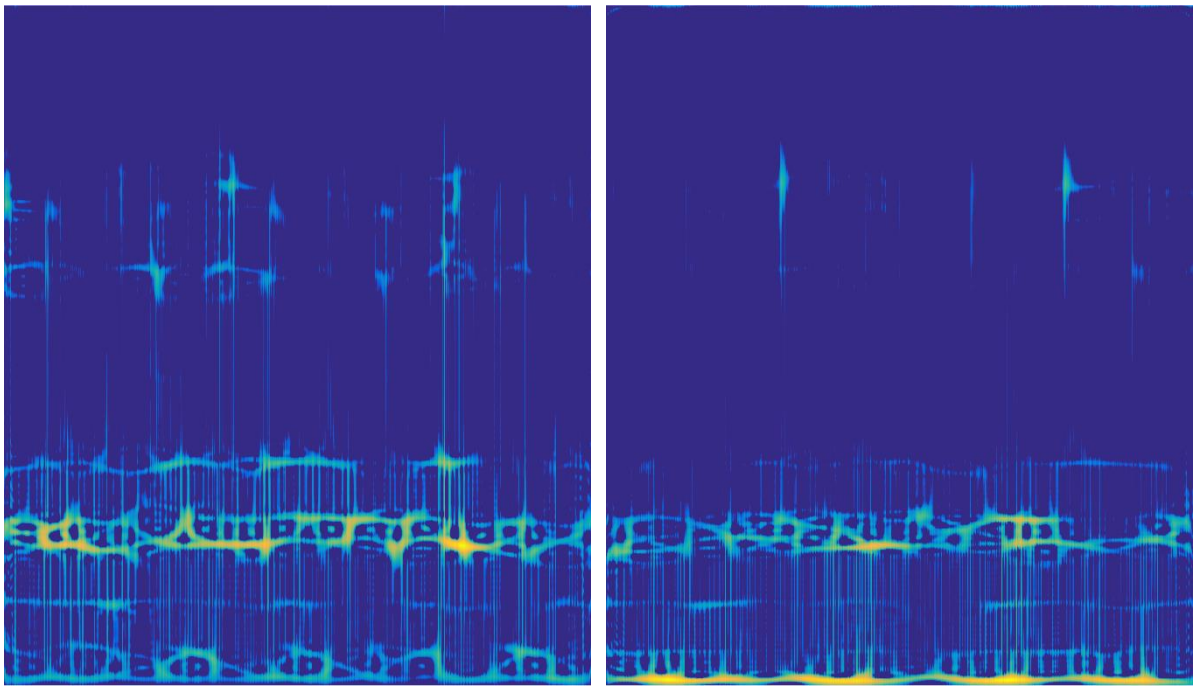

Fig. 49. BJ: normal condition (left side), blocked fuel injector in the fourth cylinder (right side).

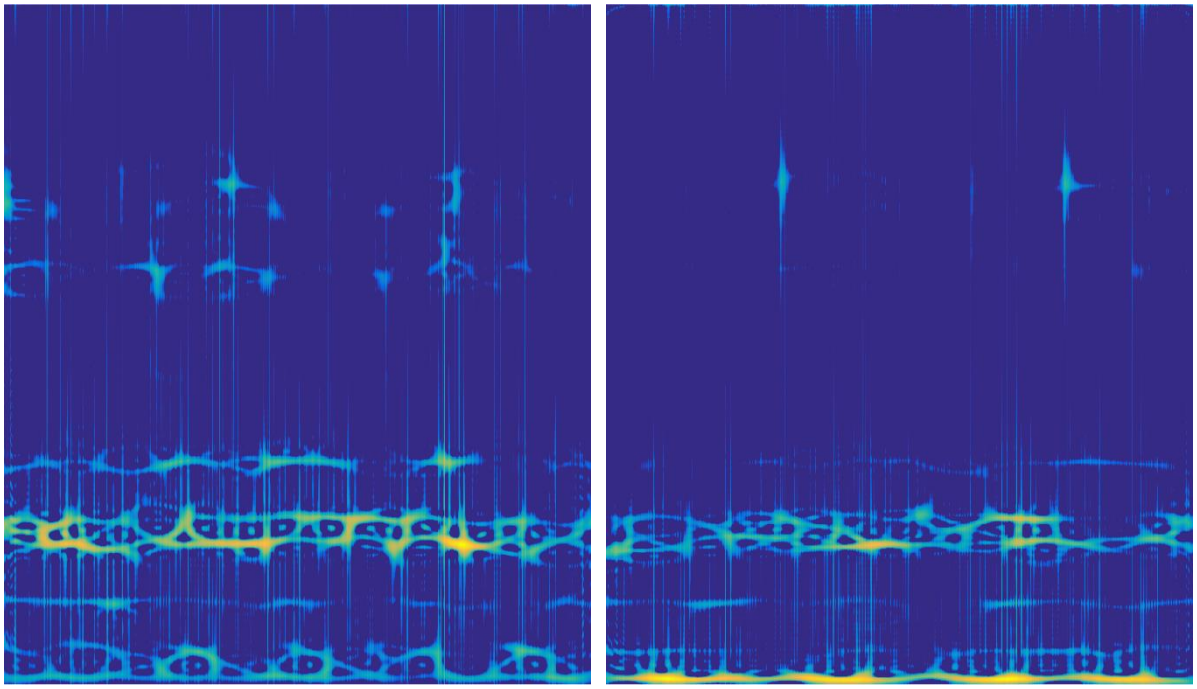

Fig. 50. BUD: normal condition (left side), blocked fuel injector in the fourth cylinder (right side).

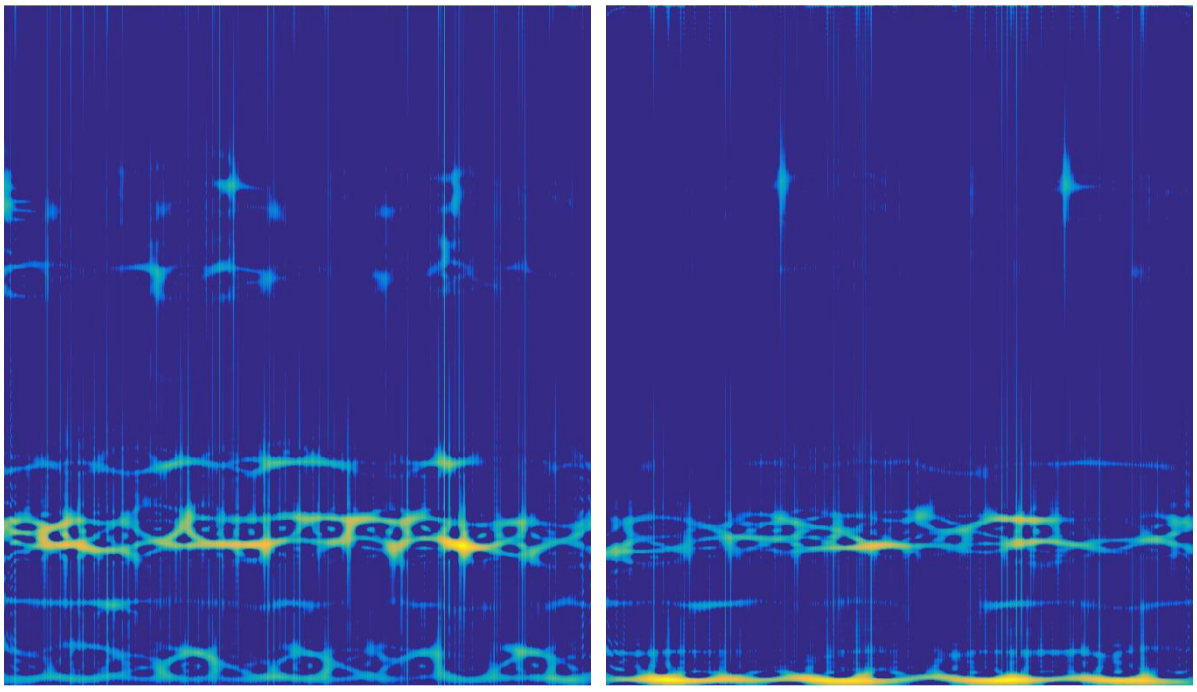

Fig. 51. CW: normal condition (left side), blocked fuel injector in the fourth cylinder (right side).

6. CONCLUSIONS AND FUTURE WORK

In this work a new non-intrusive and low-cost monitoring system for IC engines was developed, that is able to register the working hours of boat engines and detect faults. Separate prototypes modules were developed for each of these purposes, and both use vibration information. An accelerometer is used to detect the working hours of the engine in the first module, while in the second one a piezoelectric sensor is used to capture vibrations and record them during its working periods, subsequently allowing the signal analysis and fault detection. The developed BLE service provides the interface to send information from the hardware modules to the user's smartphone about accumulated engine's working hours and vibration data, allowing the execution of data analysis routines externally to the hardware modules.

6.1 CONCLUSIONS

Regarding the developed hardware, we can conclude that it serves the purposes for what it was developed for. The low power accelerometer, activated periodically, records effectively the engine's working hours (identifying the start and stop of the motor), although with a low-frequency rate vibration data signal. Because it is a low-power module, it does not jeopardize the power requirements. The piezoelectric polyvinylidene fluoride (PVDF) film, used to record the engine's vibration necessary for fault detection, because it needs an electronic circuit necessary to amplify and capture its data, is activated sparsely in time. This way, again, the power requirements are not jeopardized because of the very low activation frequency. Moreover, the piezoelectric sensor revealed to be a very accurate sensor, being able to capture all of the available vibration signals, because of its high bandwidth (1 MHz). Regarding the microprocessor and A/D converter, the maximum sampling frequency for the signal is 1M sample/s, which again is much higher than the bandwidth of the vibration signal. Note that all of the recorded signal frequencies were below 10 kHz, as it can be seen on figures 27-30.

In resume, the module used for condition monitoring showed a good performance and allowed to get reliable (enough) data for the further digital processing.

Regarding the fault detection analysis, the frequency analysis and, especially, the time domain analysis, when used alone, were not able to effectively and correctly identify the tested faults in the engine. Therefore, its application for fault detection in IC engines is very limited (when these analyses are used alone).

At the same time, some Time-Frequency methods showed promising results and seem to be better suited for this application. These TF methods were analyzed using the Rényi entropy and visual analysis assessment methods. Both assessment methods showed that, among the different tested TF methods, the Morlet scalogram was the one that was able to detect faults more easily, due to the highest absolute difference between good and faulty conditions. The visual analysis provided more accurate evaluation of methods, in comparison with Rényi entropy, as it allows to consider various unrelated characteristics at the same time. In fact, this visual analysis is in fact the human's perception used to identify different results on the faulty and non-faulty graphs. Nevertheless, the results obtained with the Rényi entropy comparison metric achieved a similar and consisting result when compared with the visual analysis of the results.

It is also important to refer that 16 TF algorithms were tested, which in combination may also be used as a fingerprint for the engine behavior, improving fault detection and enhancing the reliability of the fault detection system. However, this will be analyzed in a future work.

In resume, the results showed that it is possible to build a non-intrusive, low-priced, reliable, and compact monitoring system, independent from the engine itself, and capable of detecting faults in the engine.

6.2 FUTURE WORK

Only four faults were considered, namely: no spark on the first cylinder, no spark on the fourth cylinder, blocked fuel injector in the first cylinder is blocked, blocked fuel injector in the fourth cylinder. This means that, as future work, more and different faults should be evaluated. Also, the faults should be tested in different motors, in order to verify if similar results could be

obtained in different test scenarios and environments. By improving the variety and quantity of data available, the method for fault detection can be automated. Moreover, the use of statistical methods for data mining should also improve the fault prediction methodology.

Also as a future work, the complete system should be integrated, i.e., both developed hardware modules, as well as the app to provide the user's interface with the system. The firmware should also be completed to allow the connection between the app and the device.

Finally, while all of the above future work perspectives can be finished, a final hardware device should also be implemented, integrating and optimizing the existing hardware modules.

6.3 PUBLICATIONS MADE DURING THE THESIS

During the Master Thesis several publications were made that either resulted from the work done in this period or contributed to it, as a result of the gathered knowledge. These publications were:

- Sergey Nogin, Jorge Semião, Jânio Monteiro (2017) A non-intrusive IoT system for the Detection of Faults in Internal Combustion Engines. In Proceedings of the INCREaSE 2017, Faro, Portugal. (status: accepted)
- Sergey Nogin, Jânio Monteiro, Sergio Gómez Melgar, José Peyroteo, António Mortal, Carlos M. Santos, José Livramento, Pedro J.S. Cardoso, Jorge Semião (2017). A Platform for the Promotion of Energy Efficiency and Monitoring in Hotel Units. In Technological Developments for Cultural Heritage and eTourism Applications. IGI Global. (status: accepted).
- João Pereira, Sergey Nogin, Pedro J. S. Cardoso, and João M.F. Rodrigues. (2016). A Cultural Heritage and Points of Interest Multi-Criteria Router Supported on Visitors Preferences. In Proceedings of the 7th International Conference on Software Development and Technologies for Enhancing Accessibility and Fighting Info-exclusion (DSAI 2016). ACM, New York, NY, USA, 392-399. DOI: 10.1145/3019943.3019999.

BIBLIOGRAPHY AND REFERENCES

[1] R. Randall, Vibration-based Condition Monitoring: Industrial, Automotive and Aerospace, 1st ed. John Wiley & Sons, 2011, pp. 1-8.

[2] C. Scheffer, P. Girdhar, “Practical machinery vibration analysis and predictive maintenance, 1st ed. Oxford: Newnes, 2004, pp. 1-3, 5.

[3] R. C. Wu, J. I. Tsai, C. T. Chiang and Chen-Sen Ouyang, "Detection of induction motor operation condition by acoustic signal," 2010 8th IEEE International Conference on Industrial Informatics, Osaka, 2010, pp. 792-797.

[4] Y. L. Zhan, Z. B. Shi, T. Shwe and X. Z. Wang, "Fault Diagnosis of Marine Main Engine Cylinder Cover Based on Vibration Signal," 2007 International Conference on Machine Learning and Cybernetics, Hong Kong, 2007, pp. 1126-1130.

[5] Louis Columbus, Industrial Analytics Based On Internet Of Things Will Revolutionize Manufacturing, Forbes.com, 2017. [Online]. Available: https://www.forbes.com/sites/louiscolumbus/2016/12/03/industrial-analytics-based-on-internet-of-things-will-revolutionize-manufacturing/#5074afb16c03. [Accessed: 16- May- 2017].

[6] "How are Preventive & Predictive Maintenance Different?", eMaint web page, 2016. [Online]. Available: https://www.emaint.com/preventive-vs-predictive-maintenance/. [Accessed: 06- Jun- 2017].

[7] Honeywell, Specifying Hour Meters: Making Sound Choices, Honeywell International Inc., Whitepaper, 2007, pp. 1-2.

[8] ENM Series T60 datasheet, [Online]. Available: http://www.enmco.com/pdf/646.PDF. [Accessed: 21- May- 2017]

[9] ENM Series T15 datasheet, [Online]. Available: http://www.enmco.com/pdf/682.PDF. [Accessed: 21- May- 2017]

[10] Runleader RL-HM016B Hour Meter, [Online]. Available: http://www.run-leader.com/index.php?product/info/11/196/203/31. [Accessed: 21- May- 2017]

[11] M. Adams, Rotating machinery vibration, 1st ed. Boca Ratón (Florida): Taylor & Francis, 2010, p. 277, 284.

[12] A. Davies, Handbook of Condition Monitoring, 1st ed. Chapman & Hall, 1998, pp. 4-5, 39.

[13] Brüel & Kjær, Measuring vibration. Revised ed. K. Larson and Son, 1982, p. 7.

[14] L. Cohen, "Time-frequency distributions-a review," in Proceedings of the IEEE, vol. 77, no. 7, pp. 941-981, Jul 1989.

[15] F. Hlawatsch and G. F. Boudreaux-Bartels, "Linear and quadratic time-frequency signal representations," in IEEE Signal Processing Magazine, vol. 9, no. 2, pp. 21-67, April 1992.

[16] Z. Feng, M. Liang and F. Chu, "Recent advances in time–frequency analysis methods for machinery fault diagnosis: A review with application examples" in Mechanical Systems and Signal Processing, vol. 38, no. 1, pp. 165-205, 2013.

[17] F. Auger, P. Flandrin, P. Gonçalvès and O. Lemoine, Time-Frequency Toolbox Tutorial, 1st ed. 2005, p. 21, 126-127.

[18] M. Mufti and G. Vachtskvanos, "An intelligent approach to fault detection and identification," American Control Conference, Proceedings of the 1995, Seattle, WA, 1995, pp. 1621-1622 vol.3.

[19] J. Pons-Llinares, J. A. Antonino-Daviu, M. Riera-Guasp, S. Bin Lee, T. j. Kang and C. Yang, "Advanced Induction Motor Rotor Fault Diagnosis Via Continuous and Discrete Time–Frequency Tools," in IEEE Transactions on Industrial Electronics, vol. 62, no. 3, pp. 1791-1802, March 2015.

[20] Xiumin Yu, Le Liu, Shichun Yang, Xianglin Zhong and Derong Liu, "Misfire detection based on engine speed using wavelet," 2009 IEEE Intelligent Vehicles Symposium, Xi'an, 2009, pp. 833-837.

[21] S. V. P. S. Nidadavolu, S. K. Yadav and P. K. Kalra, "Condition monitoring of Internal Combustion engines using empirical mode decomposition and Morlet wavelet," 2009 Proceedings of 6th International Symposium on Image and Signal Processing and Analysis, Salzburg, 2009, pp. 65-72.

[22] F. Al-Badour, L. Cheded and M. Sunar, "Non-stationary vibration signal analysis of rotating machinery via time-frequency and wavelet techniques," 10th International Conference on Information Science, Signal Processing and their Applications (ISSPA 2010), Kuala Lumpur, 2010, pp. 21-24.

[23] S. M. Namburu, S. Chigusa, D. Prokhorov, L. Qiao, K. Choi and K. Pattipati, "Application of an Effective Data-Driven Approach to Real-time time Fault Diagnosis

in Automotive Engines," 2007 IEEE Aerospace Conference, Big Sky, MT, 2007, pp. 1-9.

[24] Y. Wang, Y. Xing and H. He, "An intelligent approach for engine fault diagnosis based on wavelet pre-processing neural network model," The 2010 IEEE International Conference on Information and Automation, Harbin, 2010, pp. 576-581.

[25] A. F. Aimer, A. H. Boudinar, N. Benouzza and A. Bendiabdellah, "Simulation and experimental study of induction motor broken rotor bars fault diagnosis using stator current spectrogram," 2015 3rd International Conference on Control, Engineering & Information Technology (CEIT), Tlemcen, 2015, pp. 1-7.

[26] E. H. Bouchikhi, V. Choqueuse, M. E. H. Benbouzid, J. F. Charpentier and G. Barakat, "A comparative study of time-frequency representations for fault detection in wind turbine," IECON 2011 - 37th Annual Conference of the IEEE Industrial Electronics Society, Melbourne, VIC, 2011, pp. 3584-3589.

[27] J. D. Wu and L. H. Fang, "A Fault Diagnosis System for a Mechanical Reducer Gear-Set Using Wigner-Ville Distribution and an Artificial Neural Network," 2013 13th International Conference on Computational Science and Its Applications, Ho Chi Minh City, 2013, pp. 170-173.

[28] H. Kaixing, H. Hai, Z. Jing, Z. Jianping, Z. Yangyang and L. Jiangming, "Time-frequency analysis for power transformer fault detection using vibration method," 2014 9th IEEE Conference on Industrial Electronics and Applications, Hangzhou, 2014, pp. 2110-2114.

[29] Y. Cai, S. Cheng, Y. He and P. Xu, "Application of Image Recognition Technology based on Fractal Dimension for Diesel Engine Fault Diagnosis," 2008 The 9th International Conference for Young Computer Scientists, Hunan, 2008, pp. 2948-2953.

[30] Jian-Da Wu, Peng-Hsin Chiang, "Application of Wigner–Ville distribution and probability neural network for scooter engine fault diagnosis," in Expert Systems with Applications, vol. 36, no. 2, pp. 2187-2199, 2009.

[31] S. Rajagopalan, J. A. Restrepo, J. M. Aller, T. G. Habetler and R. G. Harley, "Wigner-Ville distributions for detection of rotor faults in brushless DC (BLDC) motors operating under non-stationary conditions," 2005 5th IEEE International Symposium on Diagnostics for Electric Machines, Power Electronics and Drives, Vienna, 2005, pp. 1-7.

[32] S. Hafeez, C. S. H. Zaidi and A. Siddiqui, "Broken rotor bar detection of single phase induction motor using Wigner-Ville Distributions," 2013 IEEE 18th Conference on Emerging Technologies & Factory Automation (ETFA), Cagliari, 2013, pp. 1-7.

[33] H. Avila López, F. Martínez Cárdenas and R. González Garza, "Arterial assessment obtained from non invasive oscillometric pressure waveforms," 2013 IEEE International Autumn Meeting on Power Electronics and Computing (ROPEC), Mexico City, 2013, pp. 1-4.

[34] Hui-xing Yun and Wei-wei Zhang, "Damage detection based-propagation of the longitudinal guided wave in a bimetal composite pipe," 2011 Second International Conference on Mechanic Automation and Control Engineering, Hohhot, 2011, pp. 134-138.

[35] Andrea Volpato and Elisabetta Collini, "Time-frequency methods for coherent spectroscopy," in Optics Express, vol. 23, no. 15, pp. 20040-20050, 2015.

[36] M. Vallverdú, F. Clariá, U. Melia, A. Bayés de Luna and P. Caminal, "Measuring heart rate variability by means of information entropies based on Choi-Williams distribution," 2015 37th Annual International Conference of the IEEE Engineering in Medicine and Biology Society (EMBC), Milan, 2015, pp. 1797-1800.

[37] G. Azarnia, M. A. Tinati and R. G. Afkhami, "Heart blocks detection in ECG signals using time frequency distribution techniques," 2016 24th Iranian Conference on Electrical Engineering (ICEE), Shiraz, 2016, pp. 1568-1573.

[38] H. Teng, J. Zhao, X. Jia, Y. Jia, X. Zhang and L. Cai, "Experimental study on gearbox prognosis using total life vibration analysis," 2011 Prognostics and System Health Managment Confernece, Shenzhen, 2011, pp. 1-6.

[39] A. C. A. Figueiredo, M. F. F. Nave and E. J. Contributors, "Improved time-frequency visualization of chirping mode signals in Tokamak plasmas using the Choi-Williams distribution," in IEEE Transactions on Plasma Science, vol. 33, no. 2, pp. 468-469, Apr 2005.

[40] M. O. Mendez, M. J. Gaitan and S. Carrasco, "Time-frequency assessment of heart rate variability under Valsalva and Mueller maneuvers," Proceedings of the 25th Annual International Conference of the IEEE Engineering in Medicine and Biology Society (IEEE Cat. No.03CH37439), 2003, pp. 220-223 Vol.1.

[41] L. Estrada, A. Torres, J. Garcia-Casado, L. Sarlabous, G. Prats-Boluda and R. Jané, "Time-frequency representations of the sternocleidomastoid muscle electromyographic signal recorded with concentric ring electrodes," 2016 38th Annual International

Conference of the IEEE Engineering in Medicine and Biology Society (EMBC), Orlando, FL, 2016, pp. 3785-3788.

[42] J. Urresty, J. Riba, J. Ortega and J. Cardenas, "Stator short circuits detection in PMSM by means of Zhao-Atlas-Marks distribution and energy calculation," 2009 13th European Conference on Power Electronics and Applications, Barcelona, 2009, pp. 1-9.

[43] V. Climente-Alarcon, J. A. Antonino-Daviu, F. Vedreño-Santos and R. Puche-Panadero, "Vibration Transient Detection of Broken Rotor Bars by PSH Sidebands," in IEEE

[44] M. Thomas, R. Jacob and B. Lethakumary, "Comparison of WVD based time-frequency distributions," 2012 International Conference on Power, Signals, Controls and Computation, Thrissur, Kerala, 2012, pp. 1-8.

[45] S. Rajagopalan, J. A. Restrepo, J. M. Aller, T. G. Habetler and R. G. Harley, "Selecting time-frequency representations for detecting rotor faults in BLDC motors operating under rapidly varying operating conditions," 31st Annual Conference of IEEE Industrial Electronics Society, 2005. IECON 2005., 2005, pp. 6 pp.-.

[46] N. K. Verma, S. Goel and R. K. Sevakula, "Study of transforms and methods for their comparison," 2014 9th International Conference on Industrial and Information Systems (ICIIS), Gwalior, 2014, pp. 1-8.

[47] R. G. Baraniuk, P. Flandrin, A. J. E. M. Janssen and O. J. J. Michel, "Measuring time-frequency information content using the Rényi entropies," in IEEE Transactions on Information Theory, vol. 47, no. 4, pp. 1391-1409, May 2001.

[48] "IrDA Specifications", Irdajp.info, 2017. [Online]. Available: http://www.irdajp.info/specifications.html. [Accessed: 16- May- 2017].

[49] "Near Field Communication Technology Standards", Nearfieldcommunication.org, 2017. [Online]. Available: http://nearfieldcommunication.org/technology.html. [Accessed: 16- May- 2017].

[50] "Bluetooth Core Specification", Bluetooth.com, 2017. [Online]. Available: https://www.bluetooth.com/specifications/bluetooth-core-specification. [Accessed: 16- May- 2017].

[51] "Discover Wi-Fi Specifications", Wi-fi.org, 2017. [Online]. Available: https://www.wi-fi.org/discover-wi-fi/specifications. [Accessed: 16- May- 2017].

[52] Z. Shelby, K. Hartke, C. Bormann, The Constrained Application Protocol (CoAP), Internet Engineering Task Force (IETF), RFC7252, June 2014.

[53] OASIS. MQTT Version 3.1.1. OASIS Standard. 29 October, 2014. Retrieved January 18, 2017 from https://goo.gl/VCBTTT.

[54] "CC2650STK SimpleLink™ Bluetooth low energy/Multi-standard SensorTag | TI.com", Ti.com, 2017. [Online]. Available: http://www.ti.com/tool/cc2650stk. [Accessed: 12- Jul- 2017].

[55] "IIS328DQ - High Performance Low power 3 axis accelerometer for industrial applications - STMicroelectronics", St.com, 2017. [Online]. Available: http://www.st.com/en/mems-and-sensors/iis328dq.html. [Accessed: 12- Jul- 2017].

[56] "ADXL362 Datasheet and Product Info | Analog Devices", Analog.com, 2017. [Online]. Available: https://goo.gl/854kYR. [Accessed: 12- Jul- 2017].

[57] "DT series without leads", TE connectivity web page, 2015. [Online]. Available: http://www.te.com/usa-en/product-CAT-PFS0004.html. [Accessed: 06- Jun- 2017].

[58] "SDT1 sensor datasheet", TE connectivity web page, 2015. [Online]. Available: http://www.te.com/usa-en/product-CAT-PFS0010.html. [Accessed: 06- Jun- 2017].

[59] Measurement Specialties, Inc., "Piezo Film Sensors Technical Manual", 1999, p. 7, 25.

[60] "AB18xx - Application manual", 2017. [Online]. Available: http://www.abracon.com/Support/AppsManuals/Precisiontiming/AB18XX-Application-Manual.pdf. [Accessed: 12- Jul- 2017].

[61] "MR25H128A | Everspin", Everspin.com, 2017. [Online]. Available: https://www.everspin.com/family/mr25h128a. [Accessed: 12- Jul- 2017].

[62] "Adesto AT25SF041 datasheet", 2017. [Online]. Available: https://www.adestotech.com/wp-content/uploads/DS-AT25SF041_044.pdf. [Accessed: 12- Jul- 2017].

[63] "M95160-DRE - 16-Kbit serial SPI bus EEPROM with high speed clock 105°C operation - STMicroelectronics", St.com, 2017. [Online]. Available: http://www.st.com/en/memories/m95160-dre.html. [Accessed: 12- Jul- 2017].

[64] "FM24CL16B: 16-Kbit (2 K × 8) Serial (I2C) F-RAM | Cypress Semiconductor", Cypress.com, 2017. [Online]. Available: https://goo.gl/tNfWLS. [Accessed: 12- Jul- 2017].

[65] "CC2650MODA SimpleLink™ Bluetooth® low energy Wireless MCU Module | TI.com", Ti.com, 2017. [Online]. Available: http://www.ti.com/product/CC2650MODA. [Accessed: 12- Jul- 2017].

[66] "BL652 BLE Module | LairdTech", Lairdtech.com, 2017. [Online]. Available: https://www.lairdtech.com/products/bl652-ble-module. [Accessed: 12- Jul- 2017].

[67] "CYBLE-212019-00, CYBLE-212023-10: EZ-BLE™ PROC™ Module | Cypress Semiconductor", Cypress.com, 2017. [Online]. Available: https://goo.gl/m3S7ZW. [Accessed: 12- Jul- 2017].

[68] Agarwal, Uday et al. AN92584 - Designing For Low Power And Estimating Battery Life For BLE Applications. *C rev. Cypress, 2016. Web. 5 June 2017.

[69] J. Karki, "Signal Conditioning Piezoelectric Sensors", Texas Instruments web page, 2000. [Online]. Available: http://www.ti.com/lit/an/sloa033a/sloa033a.pdf. [Accessed: 06- Jun- 2017].

[70] "OPA703 12V, CMOS, Rail-to-Rail I/O, Operational Amplifier | TI.com", Ti.com, 2017. [Online]. Available: http://www.ti.com/product/OPA703. [Accessed: 12- Jul- 2017].

[71] "TPS60403 60mA Charge Pump Voltage Inverter with Fixed 250kHz Operation | TI.com", Ti.com, 2017. [Online]. Available: http://www.ti.com/product/TPS60403. [Accessed: 12- Jul- 2017].

[72] "Analog Discovery 2 Reference Manual", 2017. [Online]. Available: https://goo.gl/AbHVJi. [Accessed: 12- Jul- 2017].

[73] "TFTB -- Time-Frequency toolbox", Tftb.nongnu.org, 2017. [Online]. Available: http://tftb.nongnu.org. [Accessed: 22- Apr- 2017].